Deletion of GABA-B receptor in Schwann cells regulates remak bundles and small nociceptive C-fibers.

Faroni A, Castelnovo LF, Procacci P, Caffino L, Fumagalli F, Melfi S, Gambarotta G, Bettler B, Wrabetz L, Magnaghi V.
Deletion of GABA-B receptor in Schwann cells regulates remak bundles and small nociceptive C-fibers.
GLIA (2014) 62
DOI: 10.1002/glia.22625

Deletion of GABA-B receptor in Schwann cells regulates Remak bundles and small nociceptive C-fibers

Alessandro Faroni,[1,2] Luca Franco Castelnovo,[1] Patrizia Procacci,[3] Lucia Caffino,[1] Fabio Fumagalli,[1] Simona Melfi,[1] Giovanna Gambarotta,[4] Bernhard Bettler,[5] Lawrence Wrabetz,[6,7] and Valerio Magnaghi[1]

[1]*Dipartimento di Scienze Farmacologiche e Biomolecolari, Università degli Studi di Milano, Via Balzaretti 9, 20133, Milan, Italy;*
[2]*Blond McIndoe Laboratories, The University of Manchester, Institute of Inflammation and Repair, M13 9PT, Manchester, United Kingdom;*
[3]*Dipartimento di Scienze Biomediche per la Salute, Università degli Studi di Milano, Via L. Mangiagalli 14, Milan, Italy;*
[4]*Department of Clinical and Biological Sciences, Ospedale San Luigi, University of Turin, Regione Gonzole 10, 10043, Orbassano (TO), Italy;*
[5]*Department of Biomedicine, University of Basel, Klingelbergstrasse 50–70, CH-4056, Basel, Switzerland;*
[6]*Department of Genetics and Cell Biology, San Raffaele Scientific Institute, Via Olgettina 58, 20132, Milan, Italy;*
[7]*Hunter James Kelly Research Institute, School of Medicine and Biomedical Sciences, State University of New York at Buffalo, Buffalo, New York.*

Key words: sciatic nerve, non-myelinating Schwann cell, nociception, C-fibers, calcitonin gene related protein, dorsal root ganglion

Abstract

The mechanisms regulating the differentiation into non-myelinating Schwann cells is not completely understood. Recent evidence indicates that GABA-B receptors may regulate myelination and nociception in the peripheral nervous system. GABA-B receptor total knock-out mice exhibit morphological and molecular changes in peripheral myelin. The number of small myelinated fibers is higher and associated with altered pain sensitivity. Herein, we analyzed whether these changes may be produced by a specific deletion of GABA-B receptors in Schwann cells. The conditional mice (P0-GABA-B1fl/fl) show a morphological phenotype characterized by a peculiar increase in the number of small unmyelinated fibers and Remak bundles, including nociceptive C-fibers. The P0-GABA-B1fl/fl mice are hyperalgesic and allodynic. In these mice, the morphological and behavioral changes are associated with a downregulation of neuregulin 1 expression in nerves. Our findings suggest that the altered pain sensitivity derives from a Schwann cell-specific loss of GABA-B receptor functions, pointing to a role for GABA-B receptors in the regulation of Schwann cell maturation towards the non-myelinating phenotype.

Introduction

In the peripheral nervous system (PNS), the Schwann cells associate with large and medium-caliber axons in one-to-one ratio to form the myelin sheath (Webster et al., 1973). During PNS development the Schwann cells may enter another lineage, differentiating into nonmyelinating Schwann cells, which do not produce myelin but ensheath multiple small-caliber axons to form Remak bundles. The unmyelinated axons forming the Remak bundles mostly comprise the C-fibers nociceptors (about 48% of total axons in the rat sci-atic nerve) and pre/postganglionic sympathetic fibers (about 23% of total axons) (Schmalbruch, 1986).

Some factors and receptors have been implicated in axonal-Schwann cell interactions (Orita et al. 2013; Taveggia et al., 2005; Yu et al., 2009), but the biological significance of the retention of unmyelinated fibers in the PNS remains to be elucidated. Therefore, the detailed mechanisms of how Schwann cells differentiate into non-myelinating Schwann cells is still incompletely known.

C-aminobutyric acid type B (GABA-B) receptors are G-protein coupled receptors formed by the heteromeric combination of GABA-B1 and GABA-B2 subunits. By inhibiting the adenylate cyclase and calcium channels or by activating the potassium channels, GABA-B receptors mediate the effects of GABA in the nervous system (Couve et al., 2000; Ulrich and Bettler, 2007). Mice with an ablation of the GABA-B1 gene lack functional GABA-B receptors, confirm-ing the prerequisite of GABA-B1 subunits for receptor functioning (Calver et al., 2001; Schuler et al., 2001). The GABA-B1 isoforms are distributed throughout the neuronal and glial compartments in the brain, in the spinal cord (Charles et al., 2001; Margeta-Mitrovic et al., 1999) and in the dorsal root ganglion (DRG) (Campbell et al., 1993; Charles et al., 2001; Dolphin and Scott, 1986; Magnaghi, 2007; Towers et al., 2000), suggesting the involvement of GABA-B receptors in sensory functions (Bowery, 1993; Fromm, 1989; Hering-Hanit and Gadoth, 2001; Sindrup and Jensen, 2002).

The first observation on GABA and its receptors in the PNS dates back to the 80's (Bhisitkul et al., 1987; Brown et al., 1979; Brown and Marsh, 1978; Jessen et al., 1979; Morris et al., 1983; Olsen et al., 1984). GABA-B receptors were also shown in the soma of small neurons of sensory Ad and C-fibers (Desarmenien et al., 1984). Recently, we have established that the Schwann cells possess functional GABA-B receptors (Faroni et al., 2011; Magnaghi, 2007; Magnaghi et al., 2004, 2006a, 2008), which participate in the control of

Schwann cell proliferation and myelin protein expression (Magnaghi, 2007; Magnaghi et al., 2004). In particular, the lack of colocalization of GABA-B with the specific myelin associated glycoprotein suggests that GABA-B receptors are not involved in the Schwann cells committed to myelinate. Indeed, the double-staining for GABA-B1 and glial fibrillary acidic protein strengthens the preferential localization of GABA-B1 in non-myelinating Schwann cells. This was further supported by the study of the DRGs, which confirmed GABA-B1 localization in the non-myelinating Schwann cells surrounding groups of unmyelinated axons (including C-fibers) originating from small diameter DRG neurons (Procacci et al., 2012).

The GABA-B1-deficient (GABA-B1 2/2) mice (Schuler et al., 2001), with loss of functional GABA-B receptors both in neurons and glia, manifest peculiar biochemical, anatomical, and functional changes in the PNS (Magnaghi et al., 2008). The GABA-B1 2/2 nerves showed morphological and molecular alterations in the myelin, including changes in expression levels of the peripheral myelin protein 22 (PMP22) and protein zero (P0). In GABA-B1 2/2 mice the number of small myelinated fibers and small DRG neurons, usually indicating Ad-fibers, was increased as compared to wild-type. These mice have altered sensory functions (Magnaghi et al., 2008). These findings support the importance of GABA-B receptors in the peripheral myelination process and, moreover, in modulating the nociceptive fiber activity. How-ever, the contribution of neurons (e.g., the small DRG neurons) to the PNS phenotype could not be excluded.

To shed light on the peripheral GABAergic system, we investigated the role of GABA-B receptors in Schwann cells. We analyzed mice with a deletion of GABA-B1 receptors only in Schwann cells. The morphologic and morphometric analysis of the PNS (light and electron microscopy), as well as the biochemical (analysis of myelin proteins), immunohistochemical [analysis of neurofilaments (NFs), calcitonin gene related protein (CGRP) and intraepidermal nerve fibers (IENF)], the behavioral (study of gait) and the nociceptive (plantar and Von Frey tests) parameters of peripheral nerves were evaluated. We also explored the molecular mechanism upstream of the GABA-B1 control of small nociceptive C-fibers and we conclude that GABA-B receptors are important for Schwann cell commitment to a non-myelinating pheno-type during development.

Materials and Methods

Mice and Genotyping

GABA-B1$^{fl/fl}$ mice (Haller et al., 2004) were crossed with P0-CREdeleter mice (Feltri et al., 1999) to obtain P0-CRE/GABA-B1$^{fl/\ 1}$ mice, which were then back-crossed with GABA-B1$^{fl/fl}$ mice. The resulting P0-CRE/GABA-B1$^{fl/fl}$ mice, with specific deletion of GABA-B1 in Schwann cells, were chosen as experimental group (P0-GABA-B1$^{fl/fl}$), and were compared with GABA-B1$^{fl/fl}$ mice chosen as control. Experiments were conducted on 3 and 6-month-old male mice. All experiments were done according to institutional guidelines and in compliance with the policy on the use of animals approved by the European Communities Council Directive (86/609/EEC) and by the Society for Neuroscience. The genotype was determined by polymerase chain reaction (PCR) analyses on genomic DNA, extracted from tails, sciatic nerve and liver by using microLYSIS^{VR}-Plus (Microzone Limited, Haywards Heath, UK). The following primers were used: CRE1 (5^0-CCACCACCTCTCCATTGCAC-3^0), CRE2 (5^0-GCTGGCCCAAATGTT-CGTGG-3 ^{0}), P5 (5^0-TGGGGT GTGTCC TACATGCAGC-GGACGG-3^0), P6 (5^0-GCTCTTCACC TT-TCAA CCCAGCCTCAGGCAGGC-3^0), P7 (5^0-ATCTCTTCC TTGGGCT GGGTCTTT-GCTTCGCTCG-3^0), P8 (5^0-GGGTTA TTTGAATATGATCGGAATTCCTCGACT-3^0). PCR was per-formed in a standard reaction mix for the following conditions (30 cycles): 94–C for 30 s; 56 –C for 1 min; 72–C for 1 min. A final extension at 72–C for 10 min was done. The amplified products were analyzed on 1.5% agarose gels.

Schwann Cells and DRG Neurons Primary Cultures

Schwann cell cultures were obtained from sciatic nerves of 3-month-old mice. Non-nervous tissue was removed and the nerve was cut in fragments (2–3 mm each), then placed in a 35 mm petri dish with the culture medium: DMEM (Dulbecco's modified Eagle's medium) plus 10% fetal bovine serum (FBS; Life Technologies Italia, Monza, Italy), 2% insulin growth factor and 2 mM forskolin. After two weeks, the sciatic nerves were digested with 0.0625% (w/v) collagenase Type IV (Worthington Biochemical, Lakewood, NJ) and dispase (0.5 mg/mL; Life Technologies, Italia), then mechanically dissociated, filtered through a 100 mm filter (BD Biosciences, San Jose, CA) and centrifuged 5 min at 900 rpm. Pellets were resuspended in the culture medium, and then the cell suspension (6 3 10^4) was seeded on 35

mm petri dishes and grown in presence of 2 mM forskolin at 37–C, 5% CO_2, and 95% humidity.

DRG neurons cultures were obtained from the spinal cord of 3-month-old mice. The DRGs were dissociated incubating for 40 min in Ham's F12 medium (Life Technologies Italia) containing 0.125% (w/v) collagenase Type IV (Worthington Biochemical), then treated for 30 min with 0.25% (w/v) trypsin (Worthington Bio-chemical). The dissociated DRG neurons were filtered through a 100 lm membrane (BD Biosciences) and centrifuged 5 min at 500 rpm. Cells were then resuspended in Ham's F12 and purified on a gradient of 15% (w/v) bovine serum albumin (BSA; Sigma-Aldrich, Milan, Italy). Dissociated neurons were resuspended in modified Bottenstein and Sato's medium (BSM; F12 medium plus 100 lM putrescine, 30 nM sodium selenite, 20 nM progesterone, 1 mg/mL BSA, 0.1 mg/mL transferrin, and 10 pM insulin, all Sigma-Aldrich). A cell suspension (1.5 3 10^4) of DRG neurons was seeded on a 35 mm petri dish coated with poli-L-lysin and laminin (Sigma-Aldrich). After 2 h, nerve growth factor 50 ng/mL was added and the cells grown at 37–C, 5% CO_2, and 95% humidity.

Immunofluorescence and Confocal Laser Scanning Microscopy (CLSM)

Mouse sciatic nerves were fixed in 4% paraformaldehyde (PFA; Sigma-Aldrich, Milan, Italy) in phosphate buffered saline (PBS; Sigma-Aldrich) and 10 lm thick cross-sections were cut. Cells were seeded on slides, then fixed in 4% PFA and processed for immunostaining. The Schwann cell purity (more than 98%) was tested with a specific antibody against glycoprotein P0 (Magnaghi et al., 2010). The following polyclonal antibodies were used: guinea pig anti-GABA-B1 (1:300, Merk Millipore, Billerica, MA), chicken anti-CGRP (1:200, Merk Millipore), mouse monoclonal anti-NF200 kDa (1:400, Sigma-Aldrich), rabbit anti-class III b-tubulin (TUJ1, 1:300, Sigma-Aldrich). Nerve sections were incubated 30 min at room temperature in 1:500 Fluoromyelin™ red fluorescent myelin stain (Life Technologies, Italy). Nerve or cell culture slides were incubated overnight at 4–C in PBS 0.25% bovine serum albumin (Sigma-Aldrich), 0.1% Triton X-100 and the specific primary anti-body. The following day, the slides were washed two times and incu-bated 2 h at room temperature with the specific secondary labelled antibody, diluted 1:800, which was Alexa-488 or Alexa-594 (Life Technologies, Italy). After washing, slides were mounted using Vecta-shield™ (Vector Laboratories, Burlingame, CA) and nuclei stained with 4^0,6-diamidino-2-phenylindole (DAPI). Controls for the speci-ficity of antibodies included a lack of primary antibodies. Confocal microscopy was carried out using a Zeiss LSM 510 System (Gottin-gen, Germany) and

images were processed with Image Pro-Plus 6.0 (MediaCybernetics, Bethesda, MA). Quantification of the number of CGRP- and NF200-positive fibers was performed on 5 sections per genotype. At least 8 areas were randomly sampled on each section. The data were normalized to the total number of TUJ1-positive axons per field. The observer was blinded as to the genotype of the mice.

RNA Extraction and Quantitative Real-Time PCR (qRT-PCR)

Total RNA was extracted from sciatic nerves and L4–L5 DRGs of GABA-B1$^{fl/fl}$ and P0-GABA-B1$^{fl/fl}$ mice using Trizol^{TM} (Life Technologies Italia) according to the manufacturer's protocol. A mini-mum of three animals for each time point were analyzed. One microgram total RNA was subjected to a reverse transcriptase reaction and qRT-PCR for GABA-B1, ErbB2, ErbB3, neuregulin 1 (NRG1) Type I/II and Type III was performed as previously described (Ronchi et al., 2013). Primers for ErbB2 and ErbB3 were designed using Annhyb software (http://www.bioinformatics.org/ann- hyb/), while the primer sequences for NRG1 were previously reported (Ronchi et al., 2013); primer sequences for GABA-B1 were the following: forward 5^0-TCCACCAACAACAATGAGGA-3^0, reverse 5^0-GATGGC-GCAGTTCAGAGAC (Ribeiro et al., 2012). Data of the qRT-PCR experiments were analyzed using the ^{DD}Ct method for the relative quantification. The threshold cycle number (Ct) values of both the calibrator and the samples of interest were normalized to the Ct of the endogenous housekeeping gene TATA box binding protein (TBP). As calibrator we used the RNA obtained from a 3 months GABA-B1$^{fl/fl}$ sciatic nerve or DRGs, respectively.

RNAse Protection Assay (RPA)

Five micrograms for each sample of total RNA from mice sciatic nerves were processed as previously described (Magnaghi et al., 2006b). Briefly, the samples were dissolved in 20 µL hybridization solution containing [^{32}P]-labeled cRNA probes, 250,000 counts per minute (CPM) for P0 and PMP22 and 50,000 CPM for 18S, and incubated at 45°C overnight. Following incubation for 30 min at 30°C with 200 µL digestion buffer containing 1 µg/µL RNase A, and 20 U/µL RNase T1 (Sigma-Aldrich), the samples were treated for 15 min at 37–C with 10 µg proteinase K and sodium dodecyl sulfate (SDS) 20% (w/v). After phenol-chloroform extraction, the samples were separated on a 5% polyacrylamide gel, under denaturing conditions (7 mol/L urea). Following autoradiography, the levels of protected fragments for P0 and PMP22 were normalized versus 18S tRNA, and calculated by

measuring the peak densitometric area.

Western Blot

Sciatic nerves were homogenized in lysis buffer (PBS, 1% Nonidet P-40 and 1 mM EDTA; all Sigma-Aldrich) containing a cocktail of protease inhibitors (Sigma-Aldrich). Each sample (4 or 20 mg) was then dissolved in 0.1% sodium dodecyl sulfate (SDS), resolved on a 12% SDS-polyacrylamide gel electrophoresis and electroblotted to Hybond^{TM} nitrocellulose membrane (GE Healthcare Europe GmbH, Milan, Italy). After 2 h of blocking in PBS containing 1% Tween 20 and 5% dry milk, the filters were incubated 2 h with the specific primary antibody. The following polyclonal antibodies were used: guinea pig anti-GABA-B1 (1:300, Merk Millipore, Billerica, MA), rabbit anti-P0 (1:300, Sigma-Genosys, Milan, Italy), rabbit anti-PMP22 (1:200, Abcam, Cambridge, UK), rabbit anti ErbB2 (1:500, C-18, Santa Cruz Biotechnology, Dallas, TX), rabbit anti-ErbB3 (1:500, C-17, Santa Cruz Biotechnology), rabbit anti-phospho-Erk2 (1:1000, Cell Signalling, Danvers, MA), mouse anti-Erk2 (1:5000, Santa Cruz Biotechnology), mouse anti-beta-actin (1:10,000, Sigma-Aldrich), rabbit anti-alpha-tubulin (1:500, Cell Signaling). Immunoreactive proteins were then revealed with rabbit antiguinea pig or donkey antirabbit secondary antibodies coupled to horseradish peroxidase (HRP), by using the enhanced chemiluminescence (ECL; GE Healthcare Europe GmbH) method. Scanned films were analyzed densitometrically and data normalized versus alpha-tubulin or beta-actin.

Light Microscopy and Morphometry of Sciatic Nerves and DRG

Mice were perfused transcardially, under deep anesthesia, with a solution containing 2% PFA and 2% glutaraldehyde in 0.1 M sodium cacodylate buffer (Sigma-Aldrich) pH 7.3. After fixation sci-atic nerves and L4, L5 DRGs were removed and immersed in the same fixative solution overnight at 4–C. The specimens were then postfixed in 2% OsO_4 (Sigma-Aldrich), dehydrated and embedded in Epon-Araldite (Sigma-Aldrich). Semithin (0.5 lm) sections, tolui-dine blue stained were examined by light microscopy (Image Pro-Plus 6.0 software) at a final magnification of 15003. For the morphometric analysis of sciatic nerve 25 fields (corresponding to at least 25% of the total nerve cross-sectional area) were randomly selected (Mayhew and Sharma, 1984). The measurement of myelinated fibers (at least 1,500 fibers/animal) and the number of irregular shaped fibers [index of circularity (IC), calculated as squared fiber perimeter/4p fiber area, <0.75] were assessed. The morphometric analysis of

the L4, L5 DRG was performed using a model-based stereology in accordance to circle-fitting method (Pannese et al., 1997). For each ganglion about 10–12 semithin sections, obtained at a distance of 8–10 mm from each other to avoid considering the same nerve cell body profiles, were used. Since DRG neuronal cell bodies are approximately spherical and the nucleolus is within the nucleus (which is in turn located in the center of the neuron cell body), we first assessed the circularity index of neurons. Then we measured the surface area of the equatorial section of nerve cell bodies in order to estimate their volume from the radius.

Electron Microscopy and Morphometry

Ultrathin sections (ca. 70–80 nm) of the same sciatic nerves used for light microscopy, were collected on formvar coated single slot grids and counterstained with lead citrate. The specimens were examined with a Zeiss EM 10 electron microscope (Gottingen, Germany) equipped with a digital camera. To allow quantification of Remak bundles and unmyelinated axons a grid was superimposed on the merged images, counting about 90–100 fields, corresponding to 1/4 of the total nerve area. Moreover, to evaluate structural changes of myelin compaction about 20 myelinated fibers in exact cross-sections from each animal were randomly selected and photographed at a 20,000-fold magnification.

Thermal Hyperalgesia and Mechanical Allodynia

Responses to thermal and mechanical stimuli were performed on both hind paws of all mice. Heat hypersensitivity was tested according to the Hargreaves procedure (Hargreaves et al., 1988) using the Basile plantar test apparatus (Ugo Basile, Comerio, Italy). Briefly, mice were allowed to familiarize in small clear plexiglass cubicles. A constant intensity radiant heat source (beam diameter 0.5 cm and intensity 20 I.R.) was aimed at the midplantar area of the hind paw. The time from the heat source activation until paw withdrawal was recorded (in seconds). Mechanical allodynia was assessed using the dynamic plantar aesthesiometer (Ugo Basile). Mice were placed in a test cage with a wire mesh floor and the rigid tip of a Von Frey-filament (punctate stimulus) was applied to the skin, in the middle of the plantar surface of the hind paw. The filament exerted an increasing force, ranging up to 10 g in 20 s, starting below the threshold of detection and increasing until the animal removed its paw. The withdrawal threshold was expressed in grams. The with-drawal thresholds of the ipsilateral and contralateral paws were measured 4 times and the value represents the mean of the 4 evaluations.

Gait Analysis

Mice with their hind feet stained with black ink were placed on a 100 cm long gangway, which yielded 8–10 footprints per mouse. Footprints were analyzed with the Footprint 1.22 program (Klapdor et al., 1997). We evaluated the area touched by a single step, the distance between toes of fingers 1–5 and 2–4, the length of the foot step, the stride width and the stride length. Mice did not undergo any training to perform the test, moreover mice did not exhibit any contextual hyperactivity during the test.

IENF Density Analysis

IENF density was assessed in the hind paw footpad as described (Magnaghi et al., 2008). After sacrifice, 3-mm round shaped biopsies were taken from the plantar glabrous skin, then fixed in 2% PFA-lysine periodate for 24 h at 4–C. Sections (15 mm) from each foot-pad were immunostained with rabbit anti-TUJ1 (1:300, Sigma-Aldrich). The total number of TUJ1-positive fibers crossing the dermal-epidermal junction were counted and the density of IENF (IENF/mm) was calculated.

Statistical Analysis

Data were statistically evaluated by GraphPad Prism 4.00 (San Diego, CA). Statistical significance between groups was determined by means of an unpaired Student's t-test or one-way ANOVA with Tukey's post-test. P-values <0.05 were considered significant.

Results

GABA-B1 is Absent in Schwann Cells of the P0-GABA-B1$^{fl/fl}$ Mice

GABA-B1$^{fl/fl}$ mice were generated using Balb/c embryonic stem cells and maintained in the Balb/c genetic background (Haller et al., 2004). P0-CRE mice were obtained in the C57BL/6Ncrl genetic background (Feltri et al., 1999). To disrupt the GABA-B1 gene specifically in Schwann cells, mice with LoxP sites flanking the GABA-B1 gene (GABA-B1$^{fl/fl}$) were crossed with transgenic mice expressing CRE recombinase under the control of the specific Schwann cell promoter P0 (P0-CRE) (Feltri et al., 1999, 2002). A strain of mice with a Schwann cell-specific deletion of loxP-flanking the GABA-B1 sequence (Fig. 1A), the P0-GABA-B1$^{fl/fl}$ mice, was obtained.

These mice were used as the experimental group to be tested. We first characterized the cell-specific P0-GABA-B1$^{fl/fl}$ mice by analyzing the genotype.

As shown in Fig. 1B, by using a set of primers P5/P6 we selected the P0-GABA-B1$^{fl/fl}$ genotype, presenting a specific band of 740 bp that distinguishes the “floxed” allele bearing the loxP sites flanking the GABA-B sequence, from the GABA-B1$^{1/1}$ (wildtype) allele, which shows a band of 530 bp. The experimental mice (P0-GABA-B1$^{fl/fl}$) were then selected performing a PCR with a set of specific primers recognizing the P0-CRE sequence and amplifying a band of 492 bp; GABA-B1$^{fl/fl}$ mice, in which the 492 bp band was absent, were used as controls (Fig. 1B).

To confirm somatic recombination, genomic DNA from the liver or sciatic nerve of P0-GABA-B1$^{fl/fl}$ mice was analyzed by PCR using the set of primers P7/P8. As expected, liver showed a band of 1.42 kbp, while the sciatic nerve showed a broad specific band of 360 bp, resulting from the excision of the GABA-B floxed fragment in the sciatic nerve (Fig. 1B).

To assess for loss of GABA-B1 protein, we performed western blot analysis using an antibody specific for GABA-B receptor subunits. The immunoblot revealed two bands of _100 and 130 kDa, corresponding to the native forms of the GABA-B1 receptor (GABA1a and 1b), in the control GABA-B1$^{fl/fl}$ animals; the 100 kDa band almost disappeared from the P0-GABA-B1$^{fl/fl}$ nerves, whereas the 130 kDa band was still present, likely due to the residual GABA-B receptor isoform present in the neuronal/axonal compartment (Fig. 1C). The immunofluorescence analysis on transverse sections of sciatic nerve confirmed the previous data. In GABA-B1$^{fl/fl}$ control mice, positive immunoreactivity for GABA-B1 was present in the

axon, in the surrounding myelinating Schwann cells and in the non-myelinating Schwann cells. Myelin structures were stained with a myelin specific marker (Fluoromyelin^{TM} in red). In the P0-GABA-B1$^{fl/fl}$ experimental mice, staining was almost absent in the Schwann cells, while the axons showed immuno-positivity for GABA-B1, although this appeared somewhat decreased (Fig. 1D). The qRT-PCR analysis of GABA-B1 mRNA expression in DRGs; however, did not show any significant difference between P0-GABA-B1$^{fl/fl}$ and controls (0.785 6 0.040 fold expression vs. controls, 1 60.343). In contrast, the qRT-PCR confirmed the GABA-B1 drop in the sciatic nerve of P0-GABA-B1$^{fl/fl}$ mice (0.409 60.040 fold expression vs. controls, 1 6 0.162; $P < 0.01$). Furthermore, the immunofluorescence analysis of the Schwann cell primary culture from P0-GABA-B1$^{fl/fl}$ mice demonstrated that GABA-B1 disappeared specifically in Schwann cells (Fig. 1E). Indeed, a positive immunoreactivity for GABA-B1 was still present in the Schwann cell-free DRG neuron cultures either from GABA-B1$^{fl/fl}$ or P0-GABA-B1$^{fl/fl}$ mice. Immunopositivities of Schwann cells and DRG neurons are shown as separated channels in Supplemental Material of Fig. 1E.

GABA-B1 Gene Deletion Affects the Schwann Cell Phenotype and the Morphology of Peripheral Nerves

The PNS of GABA-B1-total null mice showed alterations in myelin, with morphological and molecular changes in peripheral nerves (Magnaghi et al., 2008). Therefore, we evaluated these parameters in cell-specific P0-GABA-B1$^{fl/fl}$ mice, with specific deletion of GABA-B1 receptor in Schwann cells. As expected, Schwann cells were affected, and showed signs of degeneration such as tomacula, myelin infoldings, myelin fractures, partial, and/or complete uncompaction of myelin (Fig. 2A). The extent of this effect was similar at 3 or 6 months of age, indicating an identical pattern of morphological dysregulation. The P0-GABA-B1$^{fl/fl}$ fiber profile appeared particularly irregular, either at 3 or 6 months of age. A significant increase of irregular fibers (characterized by a IC less than 0.75) was observed in 3 and 6-month-old P0-GABA-B1$^{fl/fl}$ mice, as com-pared with the GABA-B1$^{fl/fl}$ controls (Fig. 2B).

We then performed the light microscopic and morphometric analysis on sciatic nerves of P0-GABA-B1$^{fl/fl}$ mice of 3 and 6 months of age, considering all the myelinated fibers with IC > 0.75. Among the parameters analyzed, such as fiber area and myelin thickness, we observed some morphometric differences between GABA-B1$^{fl/fl}$ control and P0-GABA-B1$^{fl/fl}$ experimental mice at 3 and 6 months of age. Indeed, in 3- month-old experimental mice, the fiber area decreased (29.94 6 0.42 lm^2 control, 2,321 fibers, vs. 27.99 6 0.28 lm^2

experimental, 3,471 fibers), whereas it significantly increased (35.54 6 1.00 lm^2 control, 1,527 fibers, vs. 40.52 60.58 lm^2 experimental, 2,091 fibers) in 6-month-old mice (Fig. 3A). However, the myelin thickness rose significantly (Fig. 3B) either at 3 months (1.063 60.01 lm control vs. 1.093 60.009 lm experimental) or 6 months of age(0.983 6 0.009 lm control vs. 1.049 6 0.01 lm experimental). Therefore, it may be suggested that the changes in fiber area at both ages, 3 and 6 months, are related to a slight increase in the myelin thickness. To confirm the effects on myelin we then analyzed the gene expression and protein levels of the typical peripheral myelin proteins P0 and PMP22. The mRNA level of both genes appeared strongly increased in the experimental P0-GABA-B1$^{fl/fl}$ mice (Fig. 3C). A concomitant increase only of the P0 protein levels was observed, while the PMP22 protein levels were unchanged (Fig. 3D). The quantitative analysis (after normalization for alpha-tubulin) confirmed that in the P0-GABA-B1$^{fl/fl}$ mice the P0 protein was significantly increased by around 50 and 70%, at 3 and 6 months of age, respectively (Fig. 3D). To verify whether these myelin expression variations correlated with changes in myelin compaction we also analyzed the myelin lamellae at high magnification. The electron microscopy images disclosed lamellae uncompaction in 1.76% fibers with a predilection to affect the outer portion of the myelin sheath of P0-GABA-B1$^{fl/fl}$ 3-month-old mice (Fig. 3E). Altogether these data are intriguing because, for the first time, they demonstrate the presence of GABA-B-mediated Schwann cell-autonomous changes in peripheral nerves. The GABA-B1 deletion may affect the Schwann cell phenotype, at least in the time range between 3 (young adulthood) and 6 (middle age) months of age, thus reducing the myelination of small diameter fibers and altering myelin thickness.

The changes observed in the fiber area may be associated with a concomitant decrease in the mean axon area and diameter. Alterations in myelin, indeed, commonly produce secondary changes in axons (Scherer and Wrabetz, 2008). The morphometric analysis of axon distribution confirmed that the number of axons with diameter less than 2 lm was significantly higher in 3-month-old P0-GABA-B1$^{fl/fl}$ as compared with controls. Conversely, 6-month-old P0-GABA-B1$^{fl/fl}$ mice possess less axons with a small diameter above 2 lm, whereas control GABA-B1$^{fl/fl}$ mice have a higher number of small axons (Fig. 4A). These effects were supported by the electron microscopic images of cross-sections of sciatic nerves, showing a general decrease in the number of myelinated fibers in P0-GABA-B1$^{fl/fl}$, with an apparent increase in the number of unmyelinated fibers, both in 3 and 6-month-old mice (Fig. 4B). Considering the plasticity of Schwann cells in vivo, the changes observed in terms of size and number of small myelinated fibers in 3 and 6-month-old P0-GABA-B1$^{fl/fl}$

mice, suggested a shift from the myelinating towards the non-myelinating fate in Schwann cells. This was evaluated by per-forming the morphometric analysis of the Remak bundles and the number of axons within each Remak bundle. The non-myelinating Schwann cells, indeed, ensheath multiple small nociceptive and other axons, assembled in Remak bundles. As shown in Fig. 4C, the number of Remak bundles was significantly augmented either in 3- or in 6-month-old experimental mice as compared with controls. Moreover, the number of unmyelinated axons was also increased at 3 and 6 months in P0-GABA-B1$^{fl/fl}$ mice (Fig. 4D). Altogether these data demonstrate that the deletion of the GABA-B1 gene in Schwann cells induces changes in both Schwann cells and axons.

Small Nociceptive C-Fibers are Altered in P0-GABA-B1$^{fl/fl}$ Mice

The increased number of small axons in the PNS of P0-GABA-B1$^{fl/fl}$ mice might be indicative of volume changes in the soma of neurons in lumbar L4, L5 DRGs. Light microscopic analysis suggested that at 3 and 6 months of age, the amount of neurons with cell bodies of small size was higher in P0-GABA-B1$^{fl/fl}$ than in control mice (Fig. 5A). Morphometric analysis confirmed that the relative frequencies of small size DRG neurons (less than 15,000 mm^3) were significantly higher in P0-GABA-B1$^{fl/fl}$ than in control mice, independent of age (Fig. 5B). Conversely, the relative frequencies of large DRG neurons (from 15,000 to 45,000 mm^3) were significantly lower in P0-GABA-B1$^{fl/fl}$ than in control mice (Fig. 5B).

To check whether the modifications of the small unmyelinated fibers of P0-GABA-B1$^{fl/fl}$ mice might be related to changes in the C-fiber density in the peripheral endings, we performed the IENF analysis on hind-paw skin biopsies, which primarily assesses the density of the C-fibers. At 3 months of age, IENF density was identical in control and experimental mice (Fig. 5C). Indeed, at 6 months of age, IENF density significantly rose in P0-GABA-B1$^{fl/fl}$ experimental mice (Fig. 5C), indicating an increase of intraepidermal fibers that may participate to the changes in peripheral nociception.

Furthermore, to assess which specific types of sensory fibers were altered, we performed the immunofluorescence analysis for CGRP on sciatic nerve sections of 3 and 6-month-old P0-GABAB1$^{fl/fl}$ mice (Fig. 6A). CGRP is a neuropeptide preferentially expressed in primary afferent neurons. It conveys nociceptive stim-uli through unmyelinated C-fibers and thinly myelinated Ad fibers (Lawson, 2002; Pierce et al., 2006). As shown in Fig. 6A, we observed an apparent decrease in CGRP-positive fibers in P0-GABA-B1$^{fl/fl}$ mice. The TUJ1 antibody, a

neuronal marker that stains all axons (Draberova et al., 1998), was used for labeling all fibers and for data normalization. The merged CGRP and TUJI images revealed no changes in 3-month-old mice, while the CGRP immunopositive fibers decreased in 6-month-old P0-GABA-B1$^{fl/fl}$ experimental mice (Fig. 6A). The quantitative evaluation (Fig. 6B) confirmed a significant reduction of CGRP positive fibers only for 6-month-old experimental mice (60.60 6 6.99%) vs. control (89.50 61.56%; $P < 0.01$), while 3-month-old mice did not change: 68.67 6 4.06% control vs. 63.67 6 5.19% experimental. The decrease observed in CGRP-positive fibers may be likely ascribed to a reduction in thinly myelinated Ad fibers, rather than to changes in unmyelinated C-fibers. We also labeled fibers for NF200, a marker of all A-fibers type. As shown in Fig. 6A we did not find any qualitative or quantitative difference in the NF200 immunolabeling between control and experimental mice, neither in 3- nor in 6-month-old mice (77.33 62.19% control vs. 76.67 6 4.16% 3-month-old experimental mice; 93.01 6 1.93% control vs. 88.80 6 1.39% 6-month-old experimental mice).

P0-GABA-B1$^{fl/fl}$ Mice Develop Altered Pain Responses and Locomotor Alterations

Taken together, our results suggest that in P0-GABA-B1$^{fl/fl}$ mice, the small nociceptive fibers, mainly C-fibers ensheathed by non-myelinating Schwann cells, are altered. Therefore, we checked for the thermal (plantar test) and mechanical sensitivity (Von Frey filament) to painful stimuli in 3 and 6-month-old mice. P0-GABA-B1$^{fl/fl}$ experimental mice showed a significant reduction in thermal withdrawal latency in the acute pain test as compared with control ($P < 0.05$; Fig. 7A). This indicates a hyperalgesic state to thermal stimuli. Moreover, P0-GABA-B1$^{fl/fl}$ showed a significant reduction in mechanical allodynia to innocuous stimulation with the Von Frey filament at 3 months of age ($P < 0.05$), whereas this effect disappeared at 6 months, when no difference in paw withdrawal was seen between control and P0-GABA-B1$^{fl/fl}$ experimental mice (Fig. 7B).

We next analyzed whether the biochemical and morphological changes in PNS of P0-GABA-B1$^{fl/fl}$ mice may affect the motor function and locomotor coordination. The footprint analysis was done by the Klapdor method (Klapdor et al., 1997) on 3 and 6 month-old mice, and a representative image is shown in Fig. 7C.

The quantitative analysis was then performed (Table 1) and, among all the parameters considered (toe spread 1–5 and 2–4, length of the foot step, stride length, stride width, and area touched), two parameters were modified in the experimental mice. Indeed, the stride length (in cm) was significantly increased: 5.198 6 0.180 control vs. 6.558 60.245 ($P < 0.001$), 3 month-old experimental mice; 5.834 6 0.152 vs. 6.705 60.215 ($P < 0.05$), 6 month-old experimental mice. Additionally, the stride width (in cm) was significantly decreased in 3 month-old mice: 2.549 6 0.109 control vs. 2.244 6 0.083 experimental ($P < 0.05$). No significant changes were seen in 6-month-old mice: 2.668 60.107 control vs. 2.530 60.077 experimental (Table 1).

P0-GABA-B1$^{fl/fl}$ Mice Show Decreased NRG1 Type III Levels and Activation of ErbB/Erk2 Pathway

The neuronal EGF-like growth factor NRG1 and its tyrosine kinase ErbB receptors have emerged as key regulators of myelinating and non-myelinating Schwann cells (Chen et al.,2003, 2006; Michailov et al., 2004; Taveggia et al., 2005). We first analyzed the expression of NRG1 isoform Type III, which is the transmembrane neuronal isoform predominantly expressed during development, and the expression of the soluble isoform Type I, mainly expressed by Schwann cells. Both isoforms appeared diminished in P0-GABA-B1$^{fl/fl}$ nerves at 3 months of age (Fig. 8A,B). In particular, NRG1 Type III was significantly decreased ($P < 0.05$) to almost undetectable level (Fig. 8A). At 6 months of age neither NRG1 Type III nor Type I were unchanged in P0-GABA-B1$^{fl/fl}$ mice vs. controls (Fig. 8A,B). In parallel, the ErbB2 and ErbB3 mRNA levels were increased in P0-GABA-B1$^{fl/fl}$ mice at 3 months of age, whereas no changes were observed at 6 months (Fig. 8C,D).

ErbB3 receptor proteins (Fig. 8E). These effects were con-firmed by the immunoblot quantification that showed significant ErbB2 (178 6 11%, $P < 0.05$) and ErbB3 (1124 6 35%, P _ 0.05) increments in the sciatic nerve of P0-GABA-B1$^{fl/fl}$ mice at 3 months of age (Fig. 8F,G). No ErbB protein changes were seen at 6 months of age (Fig. 8F,G).

ErbB receptors transmit signals intracellularly through various cascades, including the mitogen-activated protein.

The immunoblots suggested also the increase of ErbB2 and kinase (MAPK)/extracellular signal-regulated kinase (Erk), whose activation suppresses Schwann cell differentiation toward the pro-myelinating/myelinating phenotype (Napoli et al., 2012; Ogata et al., 2004). The phosphorylated Erk2 (pErk2), the key effector of this pathway, was higher in P0-GABA-

B1$^{fl/fl}$ mice at 3 months of age (Fig. 8H), with no changes in the total level of Erk2 protein (Fig. 8H). The immunoblot quantification confirmed the significant increase in pErk2 (167 610%; $P < 0.05$) and ratio pErk2/totalErk (171 6 14%; $P < 0.05$), suggesting that Erk activation is dependent on ErbB receptor upregulation.

Discussion

Here we describe a previously unrevealed role for the GABA-B receptors in the regulation of non-myelinating Schwann cells and nociceptive pathways in the PNS. These cells belong to one of the major categories of Schwann cells that do not make myelin in the PNS. The factors that determine the development of mature non-myelinating Schwann cells are not yet fully elucidated. In the last decade, the involvement of neurotransmitters (e.g., adenosine triphosphate, adenosine, and acetylcholine) in the control of neuron-glial cell interaction in the PNS has received great attention (Fields and Burnstock, 2006; Loreti et al., 2007; Stevens et al., 2004). In this context, the role of the GABAergic system, whose recognition in the PNS dates back 30 years ago, has been recently reviewed (Magnaghi, 2007; Magnaghi et al., 2004, 2006a, 2008; Perego et al., 2012). Data obtained in GABA-B1 2/2 mice (total null mice) showed several biochemical, anatomical, and functional changes in the PNS. GABA-B1 2/2 mice exhibited morphological and molecular alterations in myelin, including changes in the expression of the myelin proteins P0 and PMP22, and increased number of small caliber myelinated fibers and small DRG neurons. These mice also showed changes in sensory nociceptive functions (Magna-ghi et al., 2008). More recent observations supported the GABA-B1 localization in the non-myelinating Schwann cells surrounding the unmyelinated axons (C-fibers) in the peripheral nerves (Procacci et al., 2012).

Understanding the role of the GABA-B receptors in Schwann cells and/or DRG neurons may thus be important to discern between glial or neuronal-mediated mechanisms, and may be relevant for the management of peripheral neuropathies and associated pain.

By Schwann cell-specific inactivation of GABA-B1 receptor, we showed that the GABA-B1 modulatory action in the PNS is likely Schwann cell-autonomous. The electron microscopic analysis in 3 and 6-month-old P0-GABA-B1$^{fl/fl}$ mice revealed signs of Schwann cell degeneration, such as tomacula, fractured myelin, and partial or complete uncompaction of myelin. Accordingly, also the percentage of fibers with irregular profile, an index of myelin dysregulation, was strongly augmented. Our previous findings demonstrated a GABA-B1-dependent down-regulation of P0 and PMP22 levels in naive Schwann cell cultures (Magnaghi et al., 2004), supporting the hypothesis that myelin protein expression is tonically inhibited in vivo by GABA-B receptor. In accordance, the GABA-B1 2/2 mice showed a myelin

protein overexpression (Magnaghi et al., 2008), which may contribute to the dysmyelination observed (Magyar et al., 1996; Robaglia-Schlupp et al., 2002; Wrabetz et al., 2000). Thus, a tonic disinhibition of myelin protein expression may cause the myelin changes seen in the P0-GABA-B1$^{fl/fl}$ mice. In agreement, the morphometric analysis evidenced an increase of myelin thickness in P0-GABA-B1$^{fl/fl}$ mice, underlying Schwann cell-autonomous effects and changes in myelin. However, it could be hypothesized that the observed age-dependent increase of fiber area and myelin thickness may be attributed to the relative higher number of a subset of myelinated fibers in the population considered for the morphometric analysis.

Interestingly, the morphometric analysis of P0-GABA-B1$^{fl/fl}$ mice also indicated that not only the myelin but also the axons are altered. The number and size of small fibers were changed, indicating that Schwann cell nonautonomous effects on axons also occur. The axonal changes showed a biphasic trend between adulthood (3 months) and middle aged (6 months) mice. The 3-month old P0-GABA-B1$^{fl/fl}$ mice mainly showed smaller myelinated fibers, with small axons. Instead, the 6 month-old P0-GABA-B1$^{fl/fl}$ mice presented even larger fibers, with higher caliber axons. It is known that fibers in 6-month-old mice have larger diameter than in 3-month-old mice (Sherman and Brophy, 2005). However, the myelin thickness of P0-GABA-B1$^{fl/fl}$ mice seems to be increased irrespective of mice age. Therefore, the changes observed with age may result from axonal modifications not secondary to myelin thickness, but from other Schwann cell signals independent of myelination (Rosenberg et al., 2006). This would provide further support for the hypothesis that the GABA-B receptor ablation in Schwann cells indirectly affects the neuronal compartment. In accordance, the analysis of axon distribution, as well as the count of Remak bundles and unmyelinated axons within each Remak, suggest that the P0-GABA-B1$^{fl/fl}$ mice have a higher number of small unmyelinated axons. Consistent with these observations is the increased number of small DRG neurons.

Given the plasticity of Schwann cells in vivo (Griffin and Thompson, 2008), the changes observed in small fibers of the P0-GABA-B1$^{fl/fl}$ mice suggest that the GABA-B1 receptors concur to regulate the shift towards the non-myelinating Schwann cells. This phenomenon may occur during development of perinatal nerves (Jessen and Mirsky, 2008; Woodhoo and Sommer, 2008), but in our study it affects also the mature PNS of adult mice.

In accordance with the literature, we assume that about half of the unmyelinated axons are essentially nociceptive C fibers (Coutaux et al., 2005; Schmalbruch, 1986), whose number usually correlates with the IENF density (Bickel et al., 2009). Since in P0-GABA-B1$^{fl/fl}$

mice we observed an increase in IENF density, we speculated that the thermal hyperalgesia might have been secondary to the increased number of C fibers in the skin, or to the loss of their inhibition (Wasner et al., 2004). CGRP-positive fibers mostly represent Ad and unmyelinated C-fibers (Lawson, 2002; Pierce et al., 2006). Since in P0-GABA-B1$^{fl/fl}$ mice Ad fibers were found unaffected and the number of C fibers was increased, we expected a concomitant gain in CGRP-positive fibers. Instead, in P0-GABA-B1$^{fl/fl}$ mice the CGRP-positive fibers were apparently decreased. This apparent discrepancy may have alternative explanations. The absolute amount of CGRP-positive fibers did not change in 3 and 6-month-old P0-GABA-B1$^{fl/fl}$ mice, whereas the CGRP changes seemed to occur only in control animals, in which the lack of GABA-B1 mechanisms likely did not stimulate the shift of Schwann cells from myelinating toward non-myelinating state. Overall, the major issue emerging from these observations is that the opportunity for Schwann cells to assume the myelinating or the non-myelinating phenotype may be delayed in P0-GABA-B1$^{fl/fl}$ nerves.

The gait abnormalities observed in P0-GABA-B1$^{fl/fl}$ mice, even if not similar to those previously demonstrated in GABA-B1 2/2 mice (Magnaghi et al., 2008), could be the consequence of the dysmyelination or of the painful neuropathy observed. In total null GABA-B1 2/2 mice the hyperalgesia was attributed to the sensory nerve fiber changes and/or to the impairment of central somatosensory pathways (Serra et al., 2004). It is known that GABA-B receptors are involved in regulating nociceptive pathways (Gassmann et al., 2004; Lin et al., 1996; Schuler et al., 2001), and the antinociceptive tone is partially mediated by GABA-B receptors located in the CNS, specifically in the dorsal horn of the spinal cord (Lin et al., 1996). However, our data from P0-GABA-B1$^{fl/fl}$ mice clearly indicate that the GABA-B1-mediated peripheral component is equally important in nociception.

A recent study analyzed Nav1.8-GABA-B1fl/fl mice (Gangadharan et al., 2009). These mice (also called SNS-GABA B1fl/fl) expressed the CRE recombinase under the control of the sodium channel Nav1.8 (selectively expressed in sensory neurons), thus resulting in a specific knockout of GABA-B1 receptor in DRG neurons (Agarwal et al., 2004). Although some slight modifications in response to acute inflammatory pain and in the electrophysiological analysis of Ad fibers were shown, the results from SNS-GABA-B1fl/fl mice did not suggest a clear contribution of peripherally-expressed GABA-B receptor in the regulation of pain. Differently from our model, Gangadharan et al. did not take into account the effect of age. Moreover, the cell-specific knockout of GABA-B1 in DRG affected all sensory neurons, making it impossible to distinguish between neuronal subpopulations, which

usually form the soma of functionally different afferents.

To identify GABA-B1-dependent mechanisms responsible for the changes in Schwann cell phenotype, we considered some fundamental pathways involved in Schwann cell development, such as the NRG1/ErbB signaling (Chen et al., 2003, 2006; Michailov et al., 2004; Taveggia et al., 2005). In this study, we found a GABA-B1-dependent NRG1 downregulation, particularly of the axonal form of NRG1 Type III, in accordance with the lower levels of NRG1 Type III expressed by small axons (Taveggia et al., 2005). The NRG1 Type III reduction in the experimental mice may be in line with the subsequent upregulation of ErbB2/B3 receptors, which may represent a compensatory mechanism.

Among the intracellular signaling cascades activated by ErbB receptors, the MAPK/Erk pathway acts as a negative regulator of Schwann cell differentiation versus the pro-myelinating/myelinating phenotype (Jessen and Mirsky, 2008; Napoli et al., 2012; Ogata et al., 2004). In this view, the activation of phosphorylated Erk2 isoform in P0-GABA-B1fl/fl mice may account for the instructive signal that determines the changes in nociceptive C-fibers and the biased maturation towards non-myelinating Schwann cells. However, the role of Erk1/Erk2 signaling in Schwann cells is complex and context-dependent (Napoli et al., 2012; Newbern et al., 2011); thus in P0-GABA-B1fl/fl mice other mechanisms might be taken into account.

In conclusion, our findings demonstrate that some of GABA-B1-related changes in PNS are Schwann cell-autonomous (e.g., myelin protein changes), whereas the axonal effects indicate that secondary Schwann cell nonautonomous mechanisms (e.g., changes in neurons) may occur. These effects may cause a reduction in the myelination of small diameter fibers and strengthen a role for GABA-B receptors in the maturation of Schwann cells towards the non-myelinating phenotype. The effects on non-myelinating and Remak Schwann cells are supported by several strands of data, including behavioral measures. Indeed, the effects we observed on myelination may be happening in a small subset of myelinating Schwann cells later in development that is after Remak bundles differentiation is completed.

The majority of clinical symptoms in demyelinating neuropathies are determined by the axonal atrophy secondary to the myelin damage (Hanemann and Gabreels-Festen, 2002). The comprehension of neuronal-glial interactions is fundamental for the study of the pathophysiological conditions affecting the PNS. Non-myelinating Schwann cell dysfunction could be responsible of some clinical peripheral neuropathies characterized by abnormal pain

sensitivity (Brown et al., 1980; Dutsch et al., 2002). Treatment strategies focusing on GABA-B-dependent modulation of neuropathic pain may need to target not only spinal cord or DRG neurons, but also Schwann cells in nerves.

Acknowledgment

Grant sponsor: AFM, Association Francaise Contre les Myopathies; Grant numbers: 14163-2009, 16342-2012.

The authors declare no competing financial interests. They are grateful to Marinella Ballabio and Vincenzo Conte for helpful assistance with biochemical and morphometric analysis.

References

Agarwal N, Offermanns S, Kuner R. 2004. Conditional gene deletion in primary nociceptive neurons of trigeminal ganglia and dorsal root ganglia. Genesis 38:122–129.

Bhisitkul RB, Villa JE, Kocsis JD. 1987. Axonal GABA receptors are selectively present on normal and regenerated sensory fibers in rat peripheral nerve. Exp Brain Res 66:659–663.

Bickel A, Heyer G, Senger C, Maihofner C, Heuss D, Hilz MJ, Namer B. 2009. C-fiber axon reflex flare size correlates with epidermal nerve fiber density in human skin biopsies. J Peripher Nerv Syst 14:294–299.

Bowery NG. 1993. GABAB receptor pharmacology. Annu Rev Pharmacol Tox-icol 33:109–147.

Brown DA, Adams PR, Higgins AJ, Marsh S. 1979. Distribution of gaba-receptors and gaba-carriers in the mammalian nervous system. J Physiol (Paris) 75:667–671.

Brown DA, Marsh S. 1978. Axonal GABA-receptors in mammalian peripheral nerve trunks. Brain Res 156:187–191.

Brown MJ, Sumner AJ, Greene DA, Diamond SM, Asbury AK. 1980. Distal neuropathy in experimental diabetes mellitus. Ann Neurol 8:168–178.

Calver AR, Robbins MJ, Cosio C, Rice SQ, Babbs AJ, Hirst WD, Boyfield I, Wood MD, Russell RB, Price GW, Couve A, Moss SJ, Pangalos MN. 2001. The C-terminal domains of the GABA(b) receptor subunits mediate intracellular trafficking but are not required for receptor signaling. J Neurosci 21: 1203–1210.

Campbell V, Berrow N, Dolphin AC. 1993. GABAB receptor modulation of Ca21 currents in rat sensory neurones by the G protein G(0): antisense oligo-nucleotide studies. J Physiol 470:1–11.

Charles KJ, Evans ML, Robbins MJ, Calver AR, Leslie RA, Pangalos MN. 2001. Comparative immunohistochemical localisation of GABA(B1a), GABA(B1b) and GABA(B2) subunits in rat brain, spinal cord and dorsal root ganglion. Neuroscience 106:447–467.

Chen S, Rio C, Ji RR, Dikkes P, Coggeshall RE, Woolf CJ, Corfas G. 2003. Disruption of ErbB receptor signaling in adult non-myelinating Schwann cells causes progressive sensory loss. Nat Neurosci 6:1186–1193.

Chen S, Velardez MO, Warot X, Yu ZX, Miller SJ, Cros D, Corfas G. 2006. Neuregulin 1-erbB signaling is necessary for normal myelination and sensory function. J Neurosci 26:3079–3086.

Coutaux A, Adam F, Willer JC, Le Bars D. 2005. Hyperalgesia and allodynia: Peripheral mechanisms. Joint Bone Spine 72:359–371.

Couve A, Moss SJ, Pangalos MN. 2000. GABAB receptors: A new paradigm in G protein signaling. Mol Cell Neurosci 16:296–312.

Desarmenien M, Feltz P, Occhipinti G, Santangelo F, Schlichter R. 1984. Coexistence of GABAA and GABAB receptors on A delta and C primary afferents. Br J Pharmacol 81:327–333.

Dolphin AC, Scott RH. 1986. Inhibition of calcium currents in cultured rat dorsal root ganglion neurones by (2)-baclofen. Br J Pharmacol 88:213–220.

Draberova E, Lukas Z, Ivanyi D, Viklicky V, Draber P. 1998. Expression of class III beta-tubulin in normal and neoplastic human tissues. Histochem Cell Biol 109:231–239.

Dutsch M, Marthol H, Stemper B, Brys M, Haendl T, Hilz MJ. 2002. Small fiber dysfunction predominates in Fabry neuropathy. J Clin Neurophysiol 19: 575–586.

Faroni A, Mantovani C, Shawcross SG, Motta M, Terenghi G, Magnaghi V. 2011. Schwann-

like adult stem cells derived from bone marrow and adipose tissue express gamma-aminobutyric acid type B receptors. J Neurosci Res 89:1351–1362.

Feltri ML, D'Antonio M, Previtali S, Fasolini M, Messing A, Wrabetz L. 1999. P0-Cre transgenic mice for inactivation of adhesion molecules in Schwann cells. Ann N Y Acad Sci 883:116–123.

Feltri ML, Graus Porta D, Previtali SC, Nodari A, Migliavacca B, Cassetti A, Littlewood-Evans A, Reichardt LF, Messing A, Quattrini A, Mueller U, Wrabetz L. 2002. Conditional disruption of beta 1 integrin in Schwann cells impedes interactions with axons. J Cell Biol 156:199–209.

Fields RD, Burnstock G. 2006. Purinergic signalling in neuron-glia interactions. Nat Rev Neurosci 7:423–436.

Fromm GH. 1989. The pharmacology of trigeminal neuralgia. Clin Neuro-pharmacol 12:185–194.

Gangadharan V, Agarwal N, Brugger S, Tegeder I, Bettler B, Kuner R, Kurejova M. 2009. Conditional gene deletion reveals functional redundancy of GABAB receptors in peripheral nociceptors in vivo. Mol Pain 5:68.

Gassmann M, Shaban H, Vigot R, Sansig G, Haller C, Barbieri S, Humeau Y, Schuler V, Muller M, Kinzel B, Klebs K, Schmutz M, Froestl W, Heid J, Kelly PH, Gentry C, Jaton AL, Van der Putten H, Mombereau C, Lecourtier L, Mosbacher J, Cryan JF, Fritschy JM, Luthi€ A, Kaupmann K, Bettler B. 2004. Redistribution of GABAB(1) protein and atypical GABAB responses in GABAB(2)-deficient mice. J Neurosci 24:6086–6097.

Griffin JW, Thompson WJ. 2008. Biology and pathology of non-myelinating Schwann cells. Glia 56:1518–1531.

Haller C, Casanova E, Muller M, Vacher CM, Vigot R, Doll T, Barbieri S, Gassmann M, Bettler B. 2004. Floxed allele for conditional inactivation of the GABAB(1) gene. Genesis 40:125–130.

Hanemann CO, Gabreels-Festen AA. 2002. Secondary axon atrophy and neurological dysfunction in demyelinating neuropathies. Curr Opin Neurol 15: 611–615.

Hargreaves K, Dubner R, Brown F, Flores C, Joris J. 1988. A new and sensitive method for measuring thermal nociception in cutaneous hyperalgesia. Pain 32:77–88.

Hering-Hanit R, Gadoth N. 2001. The use of baclofen in cluster headache. Curr Pain Headache Rep 5:79–82.

Jessen KR, Mirsky R. 2008. Negative regulation of myelination: Relevance for development, injury, and demyelinating disease. Glia 56:1552–1565.

Jessen KR, Mirsky R, Dennison ME, Burnstock G. 1979. GABA may be a neurotransmitter in the vertebrate peripheral nervous system. Nature 281:71–74.

Klapdor K, Dulfer BG, Hammann A, Van der Staay FJ. 1997. A low-cost method to analyse footprint patterns. J Neurosci Methods 75:49–54.

Lawson SN. 2002. Phenotype and function of somatic primary afferent noci-ceptive neurones with C-, Adelta- or Aalpha/beta-fibres. Exp Physiol 87:239– 244.

Lin Q, Peng YB, Willis WD. 1996. Role of GABA receptor subtypes in inhibition of primate spinothalamic tract neurons: difference between spinal and periaqueductal gray inhibition. J Neurophysiol 75:109–123.

Loreti S, Ricordy R, Egle De Stefano M, Augusti-Tocco G, Maria Tata A. 2007. Acetylcholine inhibits cell cycle progression in rat Schwann cells by activation of the M2 receptor subtype. Neuron Glia Biol 3:269–279.

Magnaghi V. 2007. GABA and neuroactive steroid interactions in glia: new roles for old players? Curr Neuropharmacol 5:47–64.

Magnaghi V, Ballabio M, Camozzi F, Colleoni M, Consoli A, Gassmann M, Lauria G, Motta M, Procacci P, Trovato AE, Bettler B. 2008. Altered peripheral myelination in mice lacking GABAB receptors. Mol Cell Neurosci 37:599– 609.

Magnaghi V, Ballabio M, Cavarretta IT, Froestl W, Lambert JJ, Zucchi I, Melcangi RC. 2004. GABAB receptors in Schwann cells influence proliferation and myelin protein expression. Eur J Neurosci 19:2641–2649.

Magnaghi V, Ballabio M, Consoli A, Lambert JJ, Roglio I, Melcangi RC. 2006a. GABA receptor-mediated effects in the peripheral nervous system: A cross-interaction with neuroactive steroids. J Mol Neurosci 28:89–102.

Magnaghi V, Parducz A, Frasca A, Ballabio M, Procacci P, Racagni G, Bonanno G, Fumagalli F. 2010. GABA synthesis in Schwann cells is induced by the neuroactive steroid allopregnanolone. J Neurochem 112:980–990.

Magnaghi V, Veiga S, Ballabio M, Gonzalez LC, Garcia-Segura LM, Melcangi RC. 2006b. Sex-dimorphic effects of progesterone and its reduced metabolites on gene expression of myelin proteins by rat Schwann cells. J Peripher Nerv Syst 11:111–118.

Magyar JP, Martini R, Ruelicke T, Aguzzi A, Adlkofer K, Dembic Z, Zielasek J, Toyka KV, Suter U. 1996. Impaired differentiation of Schwann cells in trans-genic mice with increased PMP22 gene dosage. J Neurosci 16:5351–5360.

Margeta-Mitrovic M, Mitrovic I, Riley RC, Jan LY, Basbaum AI. 1999. Immuno-histochemical localization of GABA(B) receptors in the rat central nervous sys-tem. J Comp Neurol 405:299–321.

Mayhew TM, Sharma AK. 1984. Sampling schemes for estimating nerve fibre size. I. Methods for nerve trunks of mixed fascicularity. J Anat 139:45–58.

Michailov GV, Sereda MW, Brinkmann BG, Fischer TM, Haug B, Birchmeier C, Role L, Lai C, Schwab MH, Nave KA. 2004. Axonal neuregulin-1 regulates myelin sheath thickness. Science

304:700–703.

Morris ME, Di Costanzo GA, Fox S, Werman R. 1983. Depolarizing action of GABA (gamma-aminobutyric acid) on myelinated fibers of peripheral nerves. Brain Res 278:117–126.

Napoli I, Noon LA, Ribeiro S, Kerai AP, Parrinello S, Rosenberg LH, Collins MJ, Harrisingh MC, White IJ, Woodhoo A, Lloyd AC. 2012. A central role for the ERK-signaling pathway in controlling Schwann cell plasticity and periph-eral nerve regeneration in vivo. Neuron 73:729–742.

Newbern JM, Li X, Shoemaker SE, Zhou J, Zhong J, Wu Y, Bonder D, Hollenback S, Coppola G, Geschwind DH, Landreth GE, Snider WD. 2011. Specific functions for ERK/MAPK signaling during PNS development. Neuron 69:91–105.

Ogata T, Iijima S, Hoshikawa S, Miura T, Yamamoto S, Oda H, Nakamura K, Tanaka S. 2004. Opposing extracellular signal-regulated kinase and Akt path-ways control Schwann cell myelination. J Neurosci 24:6724–6732.

Olsen RW, Snowhill EW, Wamsley JK. 1984. Autoradiographic localization of low affinity GABA receptors with [3H]bicuculline methochloride. Eur J Pharmacol 99:247–248.

Orita S, Henry K, Mantuano E, Yamauchi K, De Corato A, Ishikawa T, Feltri ML, Wrabetz L, Gaultier A, Pollack M, Ellisman M, Takahashi K, Gonias SL, Campana WM. 2013. Schwann cell LRP1 regulates remak bundle ultrastructure and axonal interactions to prevent neuropathic pain. J Neurosci 33: 5590–5602.

Pannese E, Barni L, Arcidiacono G, Ledda M. 1997. Cell body volume of spi-nal ganglion neurons: Estimation by three different methods. J Submicrosc Cytol Pathol 29:497–502.

Perego C, Di Cairano ES, Ballabio M, Magnaghi V. 2012. Neurosteroid allo-pregnanolone regulates EAAC1-mediated glutamate uptake and triggers actin changes in Schwann cells. J Cell Physiol 227:1740–1751.

Pierce LM, Rankin MR, Foster RT, Dolber PC, Coates KW, Kuehl TJ, Thor KB. 2006. Distribution and immunohistochemical characterization of primary afferent neurons innervating the levator ani muscle of the female squirrel monkey. Am J Obstet Gynecol 195:987–996.

Procacci P, Ballabio M, Castelnovo LF, Mantovani C, Magnaghi V. 2012. GABA-B receptors in the PNS have a role in Schwann cells differentiation? Front Cell Neurosci 6:68.

Ribeiro AF, Correia D, Torres AA, Boas GR, Rueda AV, Camarini R, Chiavegatto S, Boerngen-Lacerda R, Brunialti-Godard AL. 2012. A transcriptional study in mice with different ethanol-drinking profiles: possible involvement of the GABA(B) receptor. Pharmacol Biochem Behav 102:224–232.

Robaglia-Schlupp A, Pizant J, Norreel JC, Passage E, Saberan-Djoneidi D, Ansaldi JL, Vinay L, Figarella-Branger D, Levy N, Clarac F, Cau P, Pellissier JF, Fontes_ M. 2002. PMP22 overexpression causes dysmyelination in mice. Brain 125:2213–2221.

Ronchi G, Gambarotta G, Di Scipio F, Salamone P, Sprio AE, Cavallo F, Perroteau I, Berta GN, Geuna S. 2013. ErbB2 receptor over-expression improves post-traumatic peripheral nerve regeneration in adult mice. PLoS One 8:e56282.

Rosenberg SS, Ng BK, Chan JR. 2006. The quest for remyelination: A new role for neurotrophins and their receptors. Brain Pathol 16:288–294.

Scherer SS, Wrabetz L. 2008. Molecular mechanisms of inherited demyelinating neuropathies. Glia 56:1578–1589.

Schmalbruch H. 1986. Fiber composition of the rat sciatic nerve. Anat Rec 215:71–81.

Schuler V, Luscher C, Blanchet C, Klix N, Sansig G, Klebs K, Schmutz M, Heid J, Gentry C, Urban L, Fox A, Spooren W, Jaton AL, Vigouret J, Pozza M, Kelly PH, Mosbacher J, Froestl W, Kaslin€ E, Korn R, Bischoff S, Kaupmann K, van der Putten H, Bettler B. 2001. Epilepsy, hyperalgesia, impaired memory, and loss of pre- and postsynaptic GABA(B) responses in mice lacking GABA(B(1)). Neuron 31:47–58.

Serra J, Campero M, Bostock H, Ochoa J. 2004. Two types of C nociceptors in human skin and their behavior in areas of capsaicin-induced secondary hyperalgesia. J Neurophysiol 91:2770–2781.

Sherman DL, Brophy PJ. 2005. Mechanisms of axon ensheathment and myelin growth. Nat Rev Neurosci 6:683–690.

Sindrup SH, Jensen TS. 2002. Pharmacotherapy of trigeminal neuralgia. Clin J Pain 18:22–27.

Stevens B, Ishibashi T, Chen JF, Fields RD. 2004. Adenosine: an activity-dependent axonal signal regulating MAP kinase and proliferation in developing Schwann cells. Neuron Glia Biol 1:23–34.

Taveggia C, Zanazzi G, Petrylak A, Yano H, Rosenbluth J, Einheber S, Xu X, Esper RM, Loeb JA, Shrager P, Chao MV, Falls DL, Role L, Salzer JL. 2005. Neuregulin-1 type III determines the ensheathment fate of axons. Neuron 47: 681–694.

Towers S, Princivalle A, Billinton A, Edmunds M, Bettler B, Urban L, Castro-Lopes J, Bowery NG. 2000. GABAB receptor protein and mRNA distribution in rat spinal cord and dorsal root ganglia. Eur J Neurosci 12:3201–3210.

Ulrich D, Bettler B. 2007. GABA(B) receptors: Synaptic functions and mechanisms of diversity. Curr Opin Neurobiol 17:298–303.

Wasner G, Schattschneider J, Binder A, Baron R. 2004. Topical menthol—A human model for cold pain by activation and sensitization of C nociceptors. Brain 1271159–1271171.

Webster HD, Martin R, O'Connell MF. 1973. The relationships between inter-phase Schwann cells and axons before myelination: A quantitative electron microscopic study. Dev Biol 32:401–416.

Woodhoo A, Sommer L. 2008. Development of the Schwann cell lineage: From the neural crest

to the myelinated nerve. Glia 56:1481–1490.

Wrabetz L, Feltri ML, Quattrini A, Imperiale D, Previtali S, D'Antonio M, Martini R, Yin X, Trapp BD, Zhou L, Chiu SY, Messing A. 2000. P(0) glycoprotein overexpression causes congenital hypomyelination of peripheral nerves. J Cell Biol 148:1021–1034.

Yu WM, Yu H, Chen ZL, Strickland S. 2009. Disruption of laminin in the peripheral nervous system impedes non-myelinating Schwann cell development and impairs nociceptive sensory function. Glia 57:850–859.

Figure legends

TABLE I: Footprint Analysis of Two Parameters of Locomotor Activity of P0-GABA-B1fl/fl and GABA-B1fl/fl Mice. The stride length and width were analyzed in 3- and 6-months old mice. Data are expressed as mean of 10 mice (in cm) 6SEM. A para-metric t-test with GraphPad Prism 4.00 was used for statistical analysis. *P<0.05; ***P<0.001.

FIGURE 1: Assessment of Schwann cell-specific GABA-B1 receptor inactivation. (A) Scheme of Schwann cell inactivation obtained by crossing GABA-B1$^{fl/fl}$ mice (left) with P0-CRE mice (right) obtaining P0-GABA-B1$^{fl/fl}$ mice with specific deletion of exons VII and VIII (see Haller et al. 2004). (B) PCR images of genotyping with CRE1/CRE2, P5/P6, and P7/P8 primers. P5/P6 distinguished the P0-GABA-B1$^{fl/fl}$ (740 bp specific band) from the GABA-B1$^{1/1}$ genotype (530 bp specific band). CRE1/CRE2 distinguished the P0-GABA-B1$^{fl/fl}$ experimental mice (492 bp band) from GABA-B1$^{fl/fl}$ control mice (band was absent). P7/P8 confirmed P0-GABA-B1$^{fl/fl}$ experimental mice (360 bp band) resulting from the GABA-B floxed fragment in the sciatic nerve, whereas the liver showed a 1.42 kbp band. (C) Western blot analysis for the two native forms of the GABA-B1 receptor (i.e., GABAB1a and 1b) showed two bands of 100 and 130 kDa in GABA-B1$^{fl/fl}$ control mice. The 100 kDa band disappeared in the P0-GABA-B1$^{fl/fl}$ animals, whereas the 130 kDa band remained, likely deriving from the neuronal compartment. Alpha-tubulin (54 kDa) was used to normalize loading. (D) Immunofluorescence localization of GABA-B1 in cross-sections of P0-GABA-B1$^{fl/fl}$ sciatic nerves using CLSM. GABA-B was detected with an Alexa-488 labeled secondary antibody (green). Myelin sheaths were stained with a Fluoromyelin^{TM} specific marker (red) and nuclei were stained with dapi (blue). Merged images revealed that GABA-B1 was present in the axon, myelinating, and non-myelinating Schwann cells of control mice. In P0-GABA- B1$^{fl/fl}$ experimental mice the labeling was almost totally absent in the Schwann cells, whereas the axons were immunopositive for GABA-B1. (E) Immunofluorescence localization of GABA-B1 in Schwann cells and DRG neuron primary cultures from P0-GABA-B1$^{fl/fl}$ mice. GABA-B1 was green; P0 or TUJ specific markers for Schwann cells or neurons respectively were red; nuclei were blue. Merged images confirmed the presence of GABA-B1 in DRG neuron cultures of both strains and in Schwann cell culture of GABA-B1$^{fl/fl}$ mice, while it dis-appeared in the Schwann cells from P0-GABA-B1$^{fl/fl}$ mice. Scale bar 10 mm.

FIGURE 2: Morphological changes in myelin and Schwann cells. (A) Electron micrographs of ultrathin cross-sections of sciatic nerves. P0-GABA-B1$^{fl/fl}$ 3- and 6-month-old mice showed myelin alterations and changes in Schwann cells, such tomacula, myelin infoldings (white arrowheads), and myelin fractures (white arrows). Scale bar 5 mm. (B) The percentage of irregular fibers (considered as fibers with an IC < 0.75) was significantly higher in P0-GABA-B1$^{fl/fl}$ mice than in GABA-B1$^{fl/fl}$ controls, both at 3 months (**P < 0.01) and 6 months of age (***P < 0.001). Data were expressed as means 6SEM (5 controls, 2321 counts, 6 P0-GABA-B1$^{fl/fl}$, 3471 counts in 3-month-old mice; 5 controls, 1527 counts, 5 P0-GABA-B1$^{fl/fl}$, 2091 counts in 6-month-old mice). A parametric t-test with GraphPad Prism 4.00 was used for statistical analysis.

FIGURE 3: Myelin morphometry and expression changes in peripheral nerve. (A) Morphometric analysis of semithin cross-sections (0.5 lm) of sciatic nerves. Histograms of fiber area (in lm^2) showed a decrease in 3-month-old P0-GABA-B1$^{fl/fl}$ (***P < 0.001; n 56) and an increase in 6 month-old mice (P < 0.001; n 56), as compared with controls (n 55). All data were expressed as means 6SEM. (B) Histograms of myelin thickness (in lm) showed an increase in 3-month-old (**P < 0.01; n 56) and 6-month-old (***P < 0.001; n 56) P0-GABA-B1$^{fl/fl}$ mice as compared with controls (n 55). All data were expressed as means 6SEM. (C) Image of P0 and PMP22 mRNA levels measured by RNAse protection assay in 3- and 6-month-old mice. Sample loading was normalized vs. 18s rRNA levels. The mRNA levels of the two typical peripheral myelin proteins P0 and PMP22 appeared strongly increased in the experimental P0-GABA-B1$^{fl/fl}$ mice at both ages. (D) Image of western blot of P0 (band of 28 kDa) and PMP22 (band of 22 kDa) protein levels in 3- and 6-month-old mice. Sample loading was normalized vs. alpha-tubulin (band 54 kDa). The histograms showed the P0 and PMP22 quantification. Data were expressed as percentage of the GABA-B1$^{fl/fl}$ control expression levels after normalization to alpha-tubulin. P0 levels were significantly increased in P0-GABA-B1$^{fl/fl}$ mice as compared with controls both at 3 months (*P < 0.05) and 6 months (*P < 0.05) whereas PMP22 levels were unchanged. The experiments included 5 controls and 6 P0-GABA-B1$^{fl/fl}$ mice. All data were expressed as means 6SEM. One-way ANOVA with Tukey's post-test using GraphPad Prism 4.00 was used for statistical analysis. (E) Electron micrographs at high magnification of ultrathin cross-sections of myelinated fibers. P0-GABA-B1$^{fl/fl}$ mice showed uncompaction (white arrows) of myelin lamellae in the outer membrane. Scale bar 0.30 mm.

FIGURE 4: Assessment of axonal changes in peripheral nerve. (A) Distribution of axons with different diameters in control and P0-GABA-B1$^{fl/fl}$ 3 and 6-month-old mice. The number of axons with diameter <1 and 2 lm was significantly higher in 3-month-old P0-GABA-B1$^{fl/fl}$ mice (**P < 0.01, ***P < 0.001; 3471 counts), while the number of axons >2 lm was lower in 6-month-old P0-GABA-B1$^{fl/fl}$ mice (*P < 0.05; 2091 counts). (B) Electron microscopic images of ultrathin cross-sections of sciatic nerves of 3- and 6-month-old mice, showing a general increase in the number of unmyelinated axons in P0-GABA-B1$^{fl/fl}$ mice. Scale bar 10 mm. (C) Morphometric analysis was done on ultrathin cross-sections of sciatic nerves. Histograms of Remak bundles (number/100 mm^2) showed an increase in 3 (*P < 0.05; n 56) and 6-month-old (*P < 0.05; n 56) P0-GABA-B1$^{fl/fl}$ mice as compared with controls (n 55). All data were expressed as means 6SEM. (D) Histograms of unmyelinated axons (number/100 mm^2) showed a increase in 3-(*P < 0.05; n 56) and 6-month-old (*P < 0.05; n 56) P0-CRE/GABA-B1$^{fl/fl}$ mice as compared with controls (n 55). All data were expressed as means 6SEM. One-way ANOVA with Tukey's post-test using Graph-Pad Prism 4.00 was used for statistical analysis.

FIGURE 5: Assessment of small fiber changes in PNS. (A) Light microscopic images of semithin cross-sections (0.5 µm) of DRG stained with toluidine blue in 3- and 6-month-old mice. Neuronal somata appeared generally smaller in P0-GABA-B1$^{fl/fl}$ than in GABA-B1$^{fl/fl}$ control mice at both ages. Scale bar 20 mm. (B) Quantitative morphometric analysis of neuronal volumes (in lm^3) in control and P0-GABA-B1$^{fl/fl}$ mice. The relative frequency of small DRG neurons (<15,000 mm^3) was significantly higher in P0-GABA-B1$^{fl/fl}$ than in control mice (*P < 0.05). Conversely, the relative frequency of large DRG neurons (>15,000 mm^3) was lower in P0-GABA-B1$^{fl/fl}$ mice (**P < 0.01). Data were expressed as means of the mice analyzed (4 controls: 970 counts; 4 P0-GABA-B1$^{fl/fl}$: 1343 counts). (C) Histograms of quantitative immunocytochemistry of intraepidermal nerve fibers (IENF) density in the hind paw footpad of GABA-B1$^{fl/fl}$ (n 56) and P0-GABA-B1$^{fl/fl}$ (n 58) mice, of 3 and 6 months. A significant increase in IENF density was observed in 6-month-old P0-GABA-B1$^{fl/fl}$ (*P < 0.05). All data were expressed as means 6SEM. A parametric t-test with GraphPad Prism 4.00 was used for statistical analysis.

FIGURE 6: CGRP- and NF200-immunostaining in peripheral nerves of 3 and 6-month-old mice. (A) CLSM images of immunofluorescence localization of CGRP, NF200, and TUJ1 in cross-sections of sciatic nerves (12 lm thick). CGRP and NF200 were detected with Alexa-594 labeled secondary antibody (red). Axons were stained with an antibody recognizing the neuronal marker TUJ1 and revealed with an Alexa-488 labeled secondary antibody (green). Nuclei were stained with dapi (blue). Merged images (colocalization in yellow) suggested a CGRP decrease mainly in small unmyelinated axons of P0-GABA-B1$^{fl/fl}$ mice. No qualitative changes in NF200 were observed. Scale bar 10 mm. (B) Histograms of quantitative evaluation of CGRP immunodetection after normalization for TUJ1 positive fibers. The number of fibers was significantly decreased in 6-month-old P0-GABA-B1$^{fl/fl}$ (n 57) vs. GABA-B1$^{fl/fl}$ (n 57) control mice (**P < 0.01) while no changes were observed in 3-month-old P0-GABA-B1$^{fl/fl}$. All data were expressed as means 6SEM. A parametric t-test with GraphPadPrism 4.00 was used for statistical analysis.

FIGURE 7: Assessment of nociception and locomotor coordination. (A) Histograms of thermal nociception showing a significant reduction in paw withdrawal latency (sec) in the plantar test of 3 (*P < 0.05; n 510) and 6-month-old (*P < 0.05; n 510) P0-GABA-B1$^{fl/fl}$ mice as compared with control mice (n 510). Response latencies were assessed at infrared intensity 20. All data were expressed as mean-s 6SEM. (B) Histograms of the data from the Von Frey test. A significant reduction in mechanical allodynia to innocuous stimulation with a filament (g) was seen in 3-month-old P0-GABA-B1$^{fl/fl}$ mice (*P < 0.05; n 510). A parametric t-test with GraphPad Prism 4.00 was used for statistical analysis. (C) Representative images of footprints of 3-month-old GABA-B1$^{fl/fl}$ and P0-GABA-B1$^{fl/fl}$ mice in which the major changes were observed.

FIGURE 8: Assessment of the mechanisms downstream Schwann cell-specific GABA-B1 receptor inactivation. The relative quantification of mRNA coding for NRG1 Type III, Type I, and ErbB2/ErbB3 receptors was obtained by quantitative realtime PCR. Data were normalized to the housekeeping gene TATA box binding protein, and expressed as difference (^{DD}Ct) vs. ^{D}Ct in controls, then averaged for each experimental group (P0-GABA-B1$^{fl/fl}$, n 54; GABA-B1$^{fl/fl}$, n 54). The columns represent the 2^{-DDCt} values. (A) NRG1 Type III mRNA levels were significantly reduced in P0-GABA-B1$^{fl/fl}$ mice only at 3 months of age (**P < 0.01). (B)

NRG1 Type I gene expression did not show any statistically relevant difference either in P0-GABA-B1$^{fl/fl}$ or in GABA-B1$^{fl/fl}$ mice, at 3 and 6 months of age. (C) ErbB2 mRNA levels were significantly augmented in P0-GABA-B1$^{fl/fl}$ mice at 3 but not 6 months of age (*P < 0.05). (D) ErbB3 mRNA levels appeared unchanged either in P0-GABA-B1$^{fl/fl}$ or in GABA-B1$^{fl/fl}$ mice, at 3 and 6 months of age. (E) Representative western blot of ErbB2 (band of 180 kDa), ErbB3 (180 kDa), pErk2 (42 kDa), and Erk2 (42 kDa) proteins in 3- and 6-month-old mice. Sample loading was normalized vs. beta-actin (43 kDa). (F, G) The quantitative analysis confirmed a significant increase respectively of ErbB2 (*P < 0.05; n 54) and ErbB3 (*P < 0.05; n 54) in P0-GABA-B1$^{fl/fl}$ mice at 3 months of age, while no changes were seen at 6 months. Data are expressed as percentage 6SEM of the GABA-B1$^{fl/fl}$ control expression levels after normalization to beta-actin. (H) The quantitative evaluation of immunoblots confirmed a significantly increased Erk2 phosphorylation (*P < 0.05; n 54) with no effect on total Erk protein levels in 3-month-old P0-GABA-B1$^{fl/}$ mice. No changes in 6-month-old mice were observed. The ratio between phosphorylated and total protein levels (Erk2/b-actin, pErk2/b-actin, and Erk2/pErk2), was expressed as percentage 6SEM vs. controls. The mean value of the controls was set to 100. One-way ANOVA with Tukey's post-test using GraphPad Prism 4.00 was used for statistical analysis.

			Stride length (cm)	Stride width (cm)
3mo	10 mice	GABA-B1$^{fl/fl}$	5.198 ± 0,180	2.549 ± 0,109
			***	*
	10 mice	P0-GABA-B1$^{fl/fl}$	6.558 ± 0.245	2.244 ± 0.083
6mo	10 mice	GABA-B1$^{fl/fl}$	5.834 ± 0,152	2.668 ± 0.107
			*	
	10 mice	P0-GABA-B1$^{fl/fl}$	6.705 ± 0.215	2.530 ± 0.077

TABLE 1

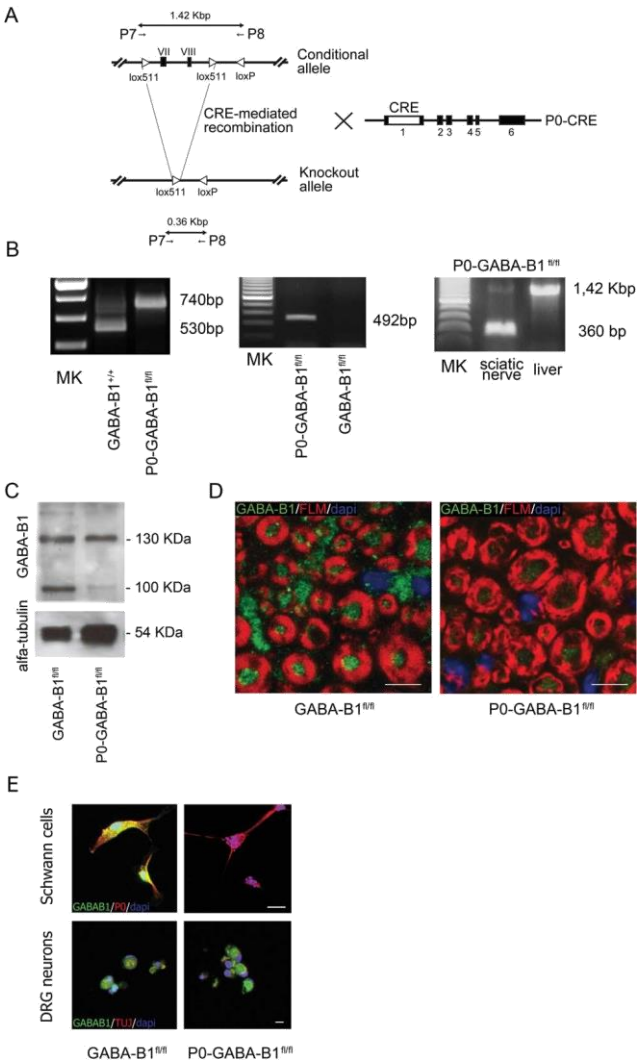
A
1.42 Kbp
P7
P8
VII
VIII
lox511
lox511
loxP
Conditional allele
CRE-mediated recombination
CRE
1
2 3
4 5
6
P0-CRE
Knockout allele
lox511
loxP
0.36 Kbp
P7
P8
B
740bp
530bp
MK
GABA-B1+/+
P0-GABA-B1fl/fl
492bp
MK
P0-GABA-B1fl/fl
GABA-B1fl/fl
P0-GABA-B1 fl/fl
1,42 Kbp
360 bp
MK
sciatic nerve
liver
C
GABA-B1
- 130 KDa
- 100 KDa
alfa-tubulin
- 54 KDa
GABA-B1fl/fl
P0-GABA-B1fl/fl
D
GABA-B1/FLM/dapi
GABA-B1/FLM/dapi
GABA-B1fl/fl
P0-GABA-B1fl/fl
E
Schwann cells
DRG neurons
GABAB1/P0/dapi
GABAB1/TUJ/dapi
GABA-B1fl/fl
P0-GABA-B1fl/fl

Figure 1

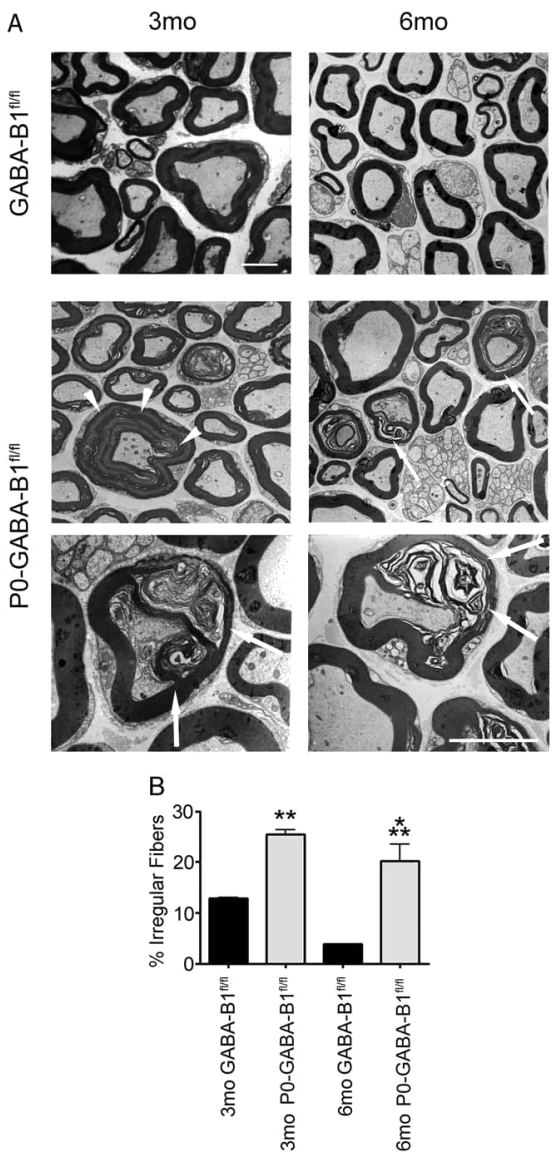
A
3mo
6mo
GABA-B1fl/fl
P0-GABA-B1fl/fl
B
% Irregular Fibers
30
20
10
0
**
**
*
3mo GABA-B1fl/fl
3mo P0-GABA-B1fl/fl
6mo GABA-B1fl/fl
6mo P0-GABA-B1fl/fl

Figure 2

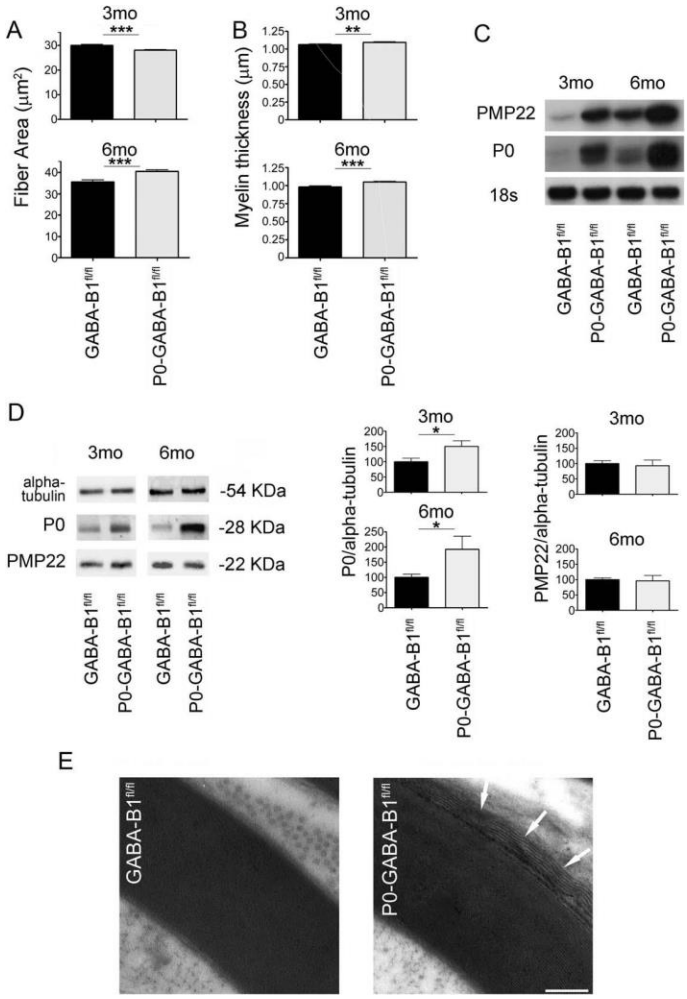
A
3mo
***
6mo
***
Fiber Area (μm²)
B
3mo
**
6mo
***
Myelin thickness (μm)
C
3mo
6mo
PMP22
P0
18s
GABA-B1fl/fl
P0-GABA-B1fl/fl
D
3mo
6mo
alpha-tubulin
P0
PMP22
-54 KDa
-28 KDa
-22 KDa
P0/alpha-tubulin
PMP22/alpha-tubulin
*
E

Figure 3

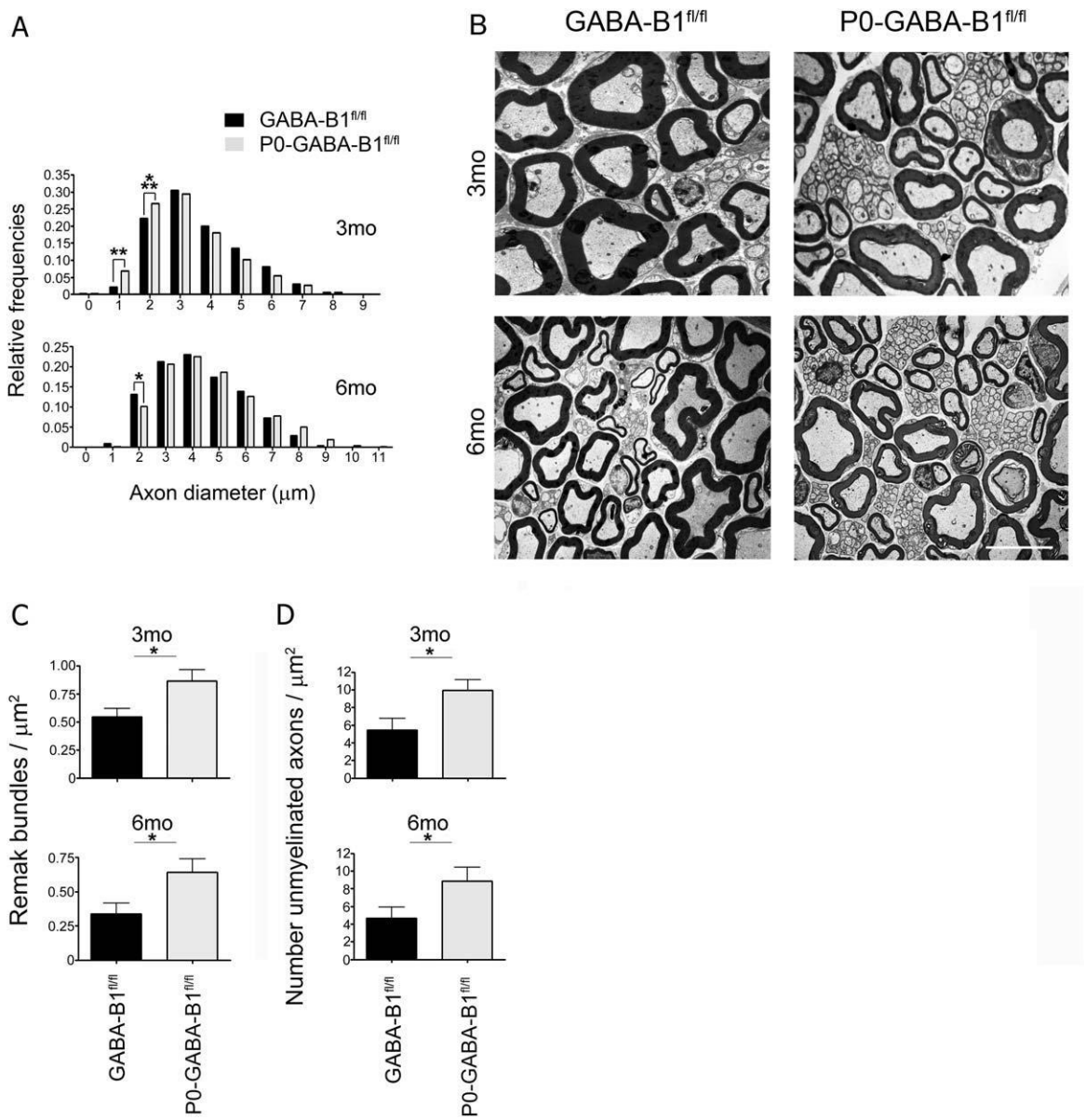
A
GABA-B1fl/fl
P0-GABA-B1fl/fl
Relative frequencies
3mo
6mo
Axon diameter (μm)
B
GABA-B1fl/fl
P0-GABA-B1fl/fl
3mo
6mo
C
Remak bundles / μm2
3mo
6mo
GABA-B1fl/fl
P0-GABA-B1fl/fl
D
Number unmyelinated axons / μm2
3mo
6mo
GABA-B1fl/fl
P0-GABA-B1fl/fl

Figure 4

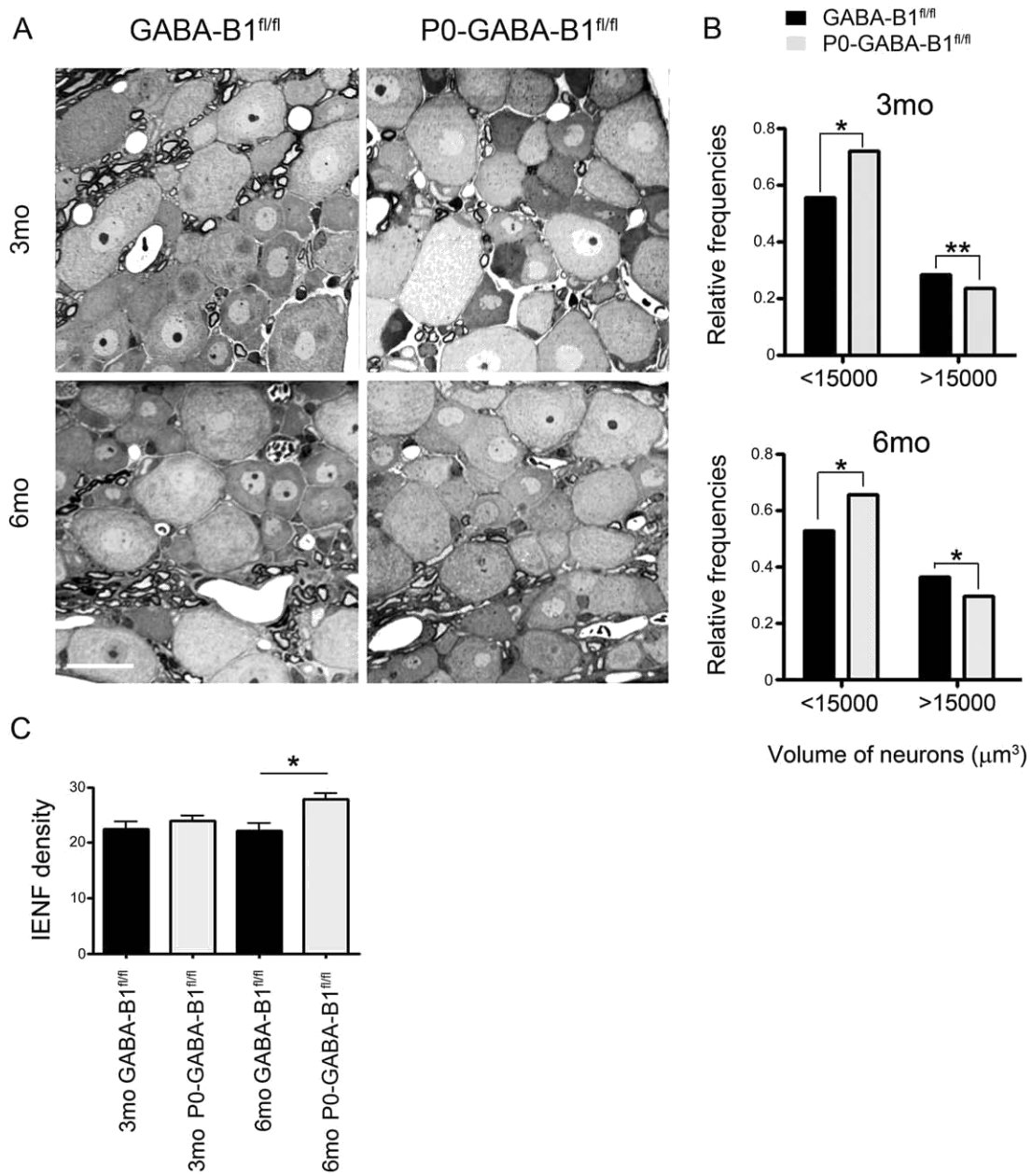
A
GABA-B1fl/fl
P0-GABA-B1fl/fl
3mo
6mo
B
GABA-B1fl/fl
P0-GABA-B1fl/fl
3mo
Relative frequencies
0.8
0.6
0.4
0.2
0
*
**
<15000
>15000
6mo
Relative frequencies
0.8
0.6
0.4
0.2
0
*
*
<15000
>15000
Volume of neurons (μm3)
C
IENF density
30
20
10
0
*
3mo GABA-B1fl/fl
3mo P0-GABA-B1fl/fl
6mo GABA-B1fl/fl
6mo P0-GABA-B1fl/fl

Figure 5

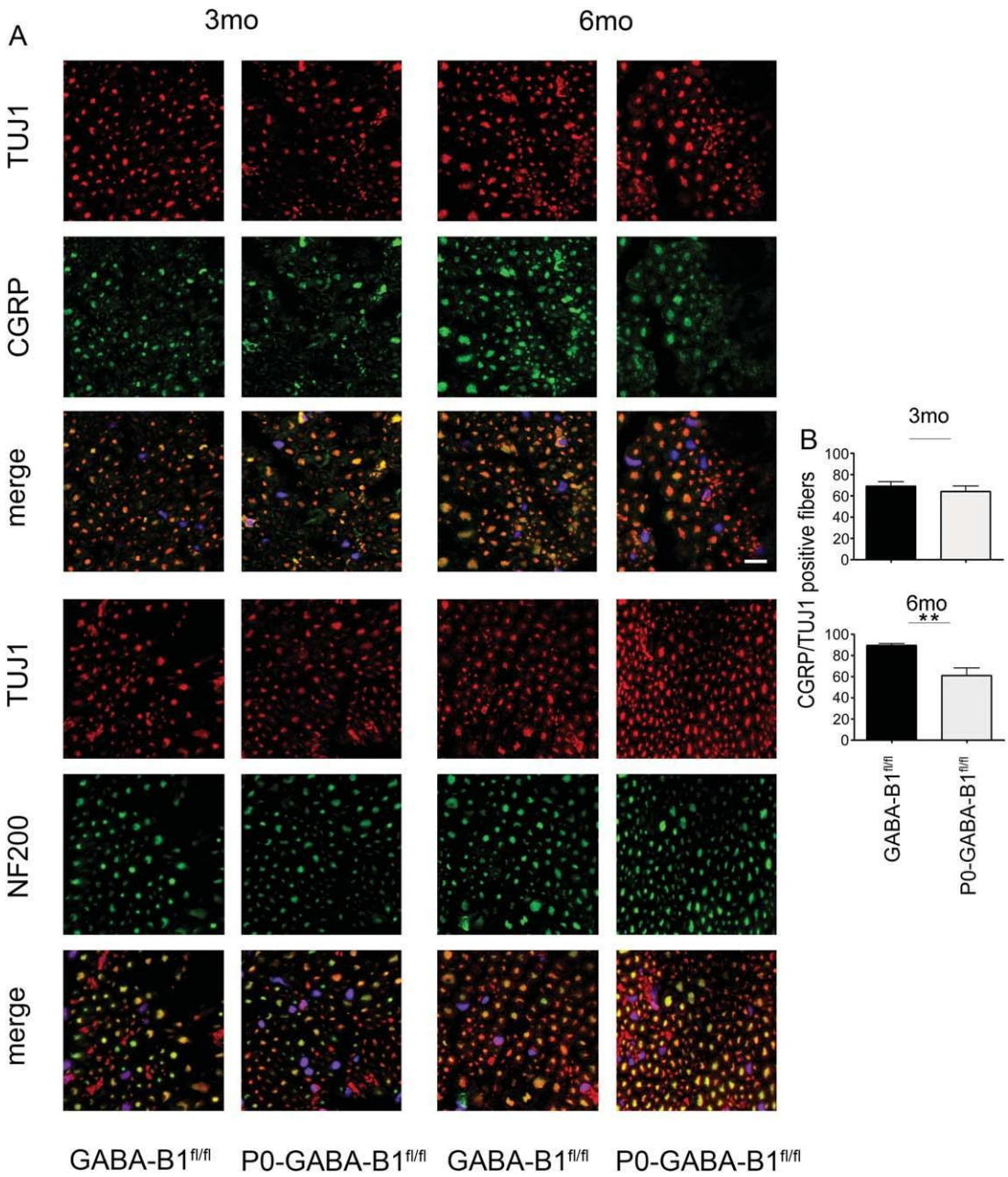
A
3mo
6mo
TUJ1
CGRP
merge
TUJ1
NF200
merge
GABA-B1fl/fl
P0-GABA-B1fl/fl
GABA-B1fl/fl
P0-GABA-B1fl/fl
B
3mo
6mo
**
CGRP/TUJ1 positive fibers
100
80
60
40
20
0
GABA-B1fl/fl
P0-GABA-B1fl/fl

Figure 6

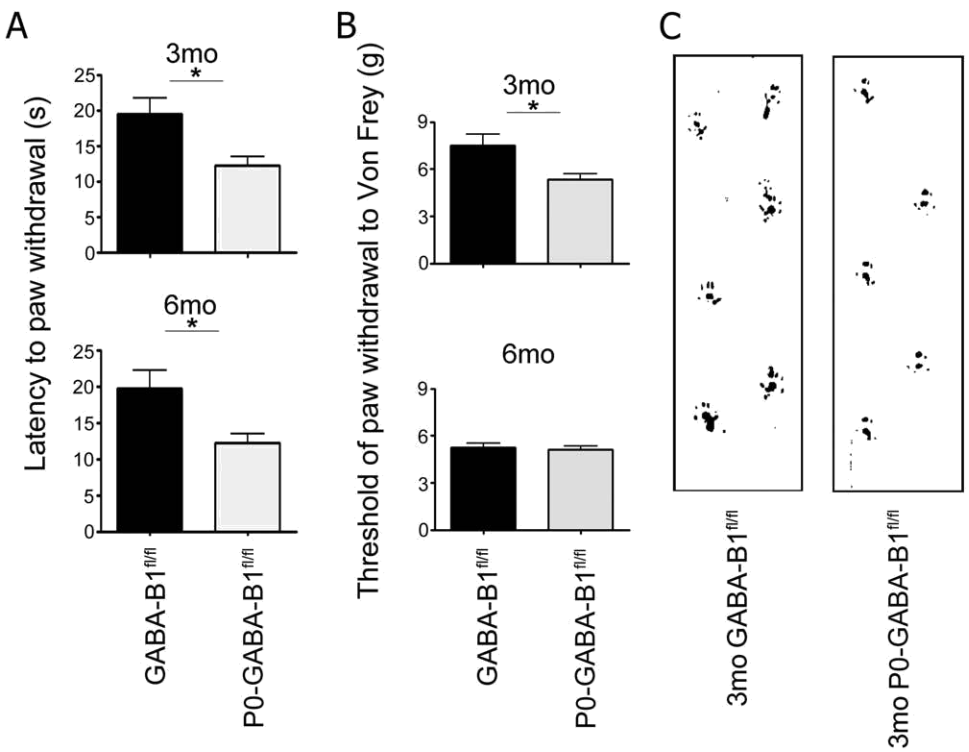
A
3mo
*
6mo
*
Latency to paw withdrawal (s)
25
20
15
10
5
0
GABA-B1fl/fl
P0-GABA-B1fl/fl
B
3mo
*
6mo
Threshold of paw withdrawal to Von Frey (g)
9
6
3
0
GABA-B1fl/fl
P0-GABA-B1fl/fl
C
3mo GABA-B1fl/fl
3mo P0-GABA-B1fl/fl

Figure 7

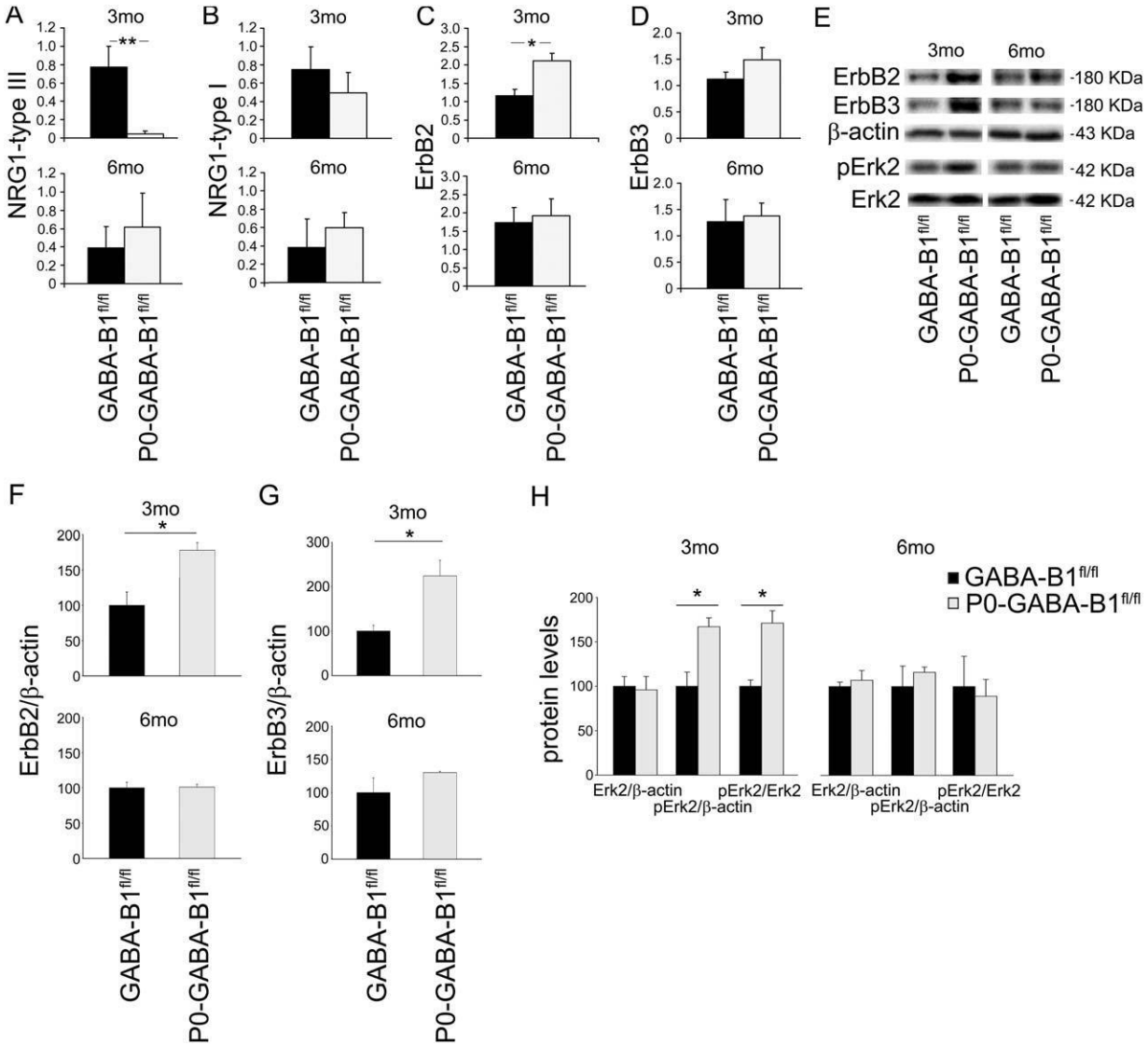
A
3mo
**
NRG1-type III
6mo
GABA-B1fl/fl
P0-GABA-B1fl/fl
B
3mo
NRG1-type I
6mo
C
3mo
*
ErbB2
6mo
D
3mo
ErbB3
6mo
E
3mo
6mo
ErbB2
ErbB3
β-actin
pErk2
Erk2
-180 KDa
-180 KDa
-43 KDa
-42 KDa
-42 KDa
F
3mo
*
ErbB2/β-actin
6mo
G
3mo
*
ErbB3/β-actin
6mo
H
3mo
6mo
GABA-B1fl/fl
P0-GABA-B1fl/fl
protein levels
Erk2/β-actin
pErk2/Erk2
pErk2/β-actin

Figure 8